外有毛細胞のmotilityに果たすモーター蛋白質の機能解明

外有毛細胞の motility に果たす モーター蛋白質の機能解明

(11307033)

平成 11 年度～平成 12 年度科学研究費補助金（基盤研究（A）（2））研究成果報告書

平成 13 年 3 月

研究代表者　　和田　仁
（東北大学大学院工学研究科教授）

外有毛細胞の motility に果たす モーター蛋白質の機能解明

(11307033)

平成 11 年度～平成 12 年度科学研究費補助金（基盤研究（A）（2））研究成果報告書

平成 13 年 3 月

研究代表者　　和田　仁
（東北大学大学院工学研究科教授）

はしがき

研究組織

研究代表者：和田　仁（東北大学大学院工学研究科教授）

研究分担者：高坂知節（東北大学大学院医学系研究科教授）

研究分担者：池田勝久（東北大学大学院医学系研究科助教授）

研究分担者：菅原路子（東北大学大学院工学研究科助手）

研究経費

平成11年度	35,300千円
平成12年度	3,500千円
計	38,800千円

研究発表

・　口頭発表

菅原路子，和田仁，臼倉寛人，局部的な外有毛細胞側壁の弾性特性解明，第10回バイオエンジニアリング講演会・秋季セミナー，1999年10月2日

菅原路子，和田仁，外有毛細胞に存在すると推察されるタンパク質モータの分布，第10回日本耳科学会学術講演会，2000年10月19日

Contents

Abstract

It is well established that the isolated outer hair cell (OHC) can elongate and contract in response to an electrical stimulation. This electromotility is suggested to produce the force and affect the basilar membrane motion. As a result, the force production of the OHC presumably leads to the fine tuning of the mammalian cochlea. As the electromotility would arise from a conformational change of molecules "protein motors" and they might distribute along the OHC lateral wall, the force generated by the OHC electromotility would be related to the mechanical properties of the lateral wall. Therefore,to evaluate the OHC's ability to influence the basilar membrane motion and tuning, it is important to understand the mechanical property of the OHC lateral wall and the distribution of protein motors. However, they are not clear.

In this study, firstly, in order to understand the difference in the stiffness along the cell axis, the local deformation of the OHC in response to the hypotonic stimulation is analyzed by measuring the displacement of the microspheres attached randomly to the cell lateral wall. Then, in order to understand the distribution of the protein motor along the cell axis, the local elongation and contraction of the OHC in response to sinusoidal voltage stimulation are analyzed by measuring the displacement of the microspheres in the same way as the case of the hypotonic stimulation. Finally, the ultrastructure of the OHC lateral wall is investigated under near physiological conditions by an atomic force microscopy, and the relationship between the difference in the stiffness along the cell axis and the ultrastructure which is observed from the AFM imaging is discussed.

1. Background and introduction

1.1. Background

1.1.1. Cochlear function

The schema of human auditory system is shown in Fig. 1.1. The auditory system is divided into external ear, middle ear and inner ear. The sound entering the external auditory canal vibrates the tympanic membrane. This vibration is mechanically transmitted by the ossicles (malleus, incus and stapes) to the cochlea (Fig. 1.2). Vibrations of the stapes generate movement of the cochlear fluids, which interact with the stiffness of the basilar membrane (BM), and produce progressive traveling wave on the BM. Figure 1.3 displays that the traveling waves on the BM have a peak near the base when high frequency sounds enter the cochlear, while low frequency sounds develop the traveling waves on the BM which has a peak near the apex. There is the organ of Corti on the BM, and it contains an array of supporting cells, outer hair cells and inner hair cells (Fig. 1.4). When the sound enters the ear, the organ of Corti has a bending motion. This bending motion generates the movement of the fluids in the space between the undersurface of the tectorial membrane and the reticular lamina, which leads to the deflection of the stereocilia of the IHCs (Fig. 1.5). By this deflection, the potential in the IHCs is changed and the transmitter is released. As a result, action potential is produced in the auditory nerve fiber. Owing to this mechanism, we can finally hear the sounds.

1.1.2. Outer hair cell (OHC)

The outer hair cell (OHC) is cylindrical shaped with a radius of 4-5 μm and a length of 30 - 90 μm (Fig. 1.6). It is capped by the cuticular plate with stereocilia at the apical end and by the synaptic membrane at the basal end. As the cuticular plate is composed of a dense network of actin filaments, it is presumed to give the

plate considerable rigidity. The OHC lateral wall consists of three layers: plasma membrane, cortical lattice and subsurface cisternae (Fig. 1.7). The cortical lattice is located between the subsurface cisternae and it consists of two types of filaments: actin and spectrin (Holley and Ashmore, 1990). Actins, which are arranged circumferentially, are 5-8 nm in diameter and are cross-linked at regular intervals by thinner spectrins, 2-4 nm in diameter (Holley and Ashmore, 1988a; 1990a; 1990b; Arima et al., 1991). The outermost plasma membrane is linked to the cortical lattice by the pillars and contains a high density of membrane particles (Arima et al., 1991; Forge, 1991). The innermost subsurface cisternae are known to be much more fluid than the plasma membrane.

As the stereocilia has the ion channel, the intracellular potential is depolarized and hyperpolarized while the stereocilia is bending *in vivo*. When the intracellular potential is depolarized, the OHC contracts. On the other hand, the OHC elongates when the intracellular potential is hyperpolarized (Fig. 1.8). This OHC motility is thought to be associated with the conformational changes of the membrane particles, which are called "motor protein." Recently, Zheng et al. indicated the gene that codes for a specialized motor protein which produces the motility, and designated it "Prestin."

1.1.3. Cochlear amplification

When the organ of Corti undergoes a bending motion, the stereocilia of the OHCs bends due to the shear motion between the tectorial membrane and the reticular lamina (Fig. 1.9). This bending of the stereocilia induces the OHCs motility. As the force produced by the OHCs motility magnifies the deflection of the organ of Corti, the movement of the fluids in the space near the stereocilia of the IHCs and the deflection of the IHC stereocilia increases. Owing to the mechanism mentioned

above, our auditory system is characterized by high sensitivity and sharp tuning.

1.2. Introduction

It is well established that the isolated outer hair cell (OHC) can elongate and contract in response to an electrical stimulation (Brownell et al., 1985; Kachar et al., 1986; Zenner, 1986; Ashmore, 1987; Santos-Sacchi and Dilger, 1988). *In vivo*, the OHC is located between the reticular lamina and Deiters' cell on the basilar membrane, and it is considered that the force produced by the OHC, which accompanies its motility, affects the basilar membrane motion. As a result, the force production of the OHC presumably leads to the fine tuning of the mammalian cochlea.

It has been reported that the OHC length changes were still evoked by changing membrane potential via a patch electrode in the whole cell when the cell was digested by internally perfusing the cytoplasm with trypsin (Kalinec et al., 1992). The same experiment was also done by Huang and Santos-Sacchi (1994) and the destruction of the cortical lattice and the subsurface cisternae by trypsin was confirmed by electron microscopy. Based on these experimental findings and microscopic study of membrane particles which were clearly visualized in the lateral plasma membrane (Forge, 1991; Kalinec et al., 1992), the OHC motility is thought to be associated with the conformational changes of membrane particles, called motor proteins. This is evidenced by the whole-cell patch-pipette recording, which confirms the existence of a nonlinear gating charge movement or a nonlinear capacitance (Santos-Sacchi, 1991). Recently, Zheng et al. (2000) identified the gene that codes for a specialized motor protein which produced the motility and designated it "Prestin." When prestin was expressed in the cultured human kidney cells, the cell showed motile response and nonlinear capacitance (Zheng et al., 2000). Therefore, prestin is the motor protein

and it may be distributed along the OHC lateral wall.

To evaluate the OHC's ability to influence the basilar membrane motion and tuning, it is important to understand the mechanical property of the OHC lateral wall and the distribution of protein motors. It has been reported that the longitudinal whole cell stiffness was measured from the length change of the OHC in response to the external stimulus is in the range of 0.8 - 25 mN/m (Zenner et al., 1992; Hallworth, 1995). However, as the structural difference exists between the apical part which has the cuticular plate and the basal part which has a half spherical shape (Fig. 1.6), there is a possibility that the local stiffness in the specific region of the OHC would be different from that in the other regions. Besides, although it has been reported that protein motors distribute in the restricted area of the cell (Holley, et al., 1988b; Evans, 1990; Hallworth, et al., 1993), the detail of the restricted area and distribution of the protein motors are not clear.

In this study, firstly, in order to understand the difference in the stiffness along the cell axis, the local deformation of the OHC in response to the hypotonic stimulation is analyzed by measuring the displacement of the microspheres attached randomly to the cell lateral wall. Then, in order to understand the distribution of the protein motor along the cell axis, the local elongation and contraction of the OHC in response to sinusoidal voltage stimulation are analyzed by measuring the displacement of the microspheres in the same way as the case of the hypotonic stimulation. Finally, the ultrastructure of the OHC lateral wall is investigated under near physiological conditions by an atomic force microscopy, and the relationship between the difference in the stiffness along the cell axis and the ultrastructure which is observed from the AFM imaging is discussed.

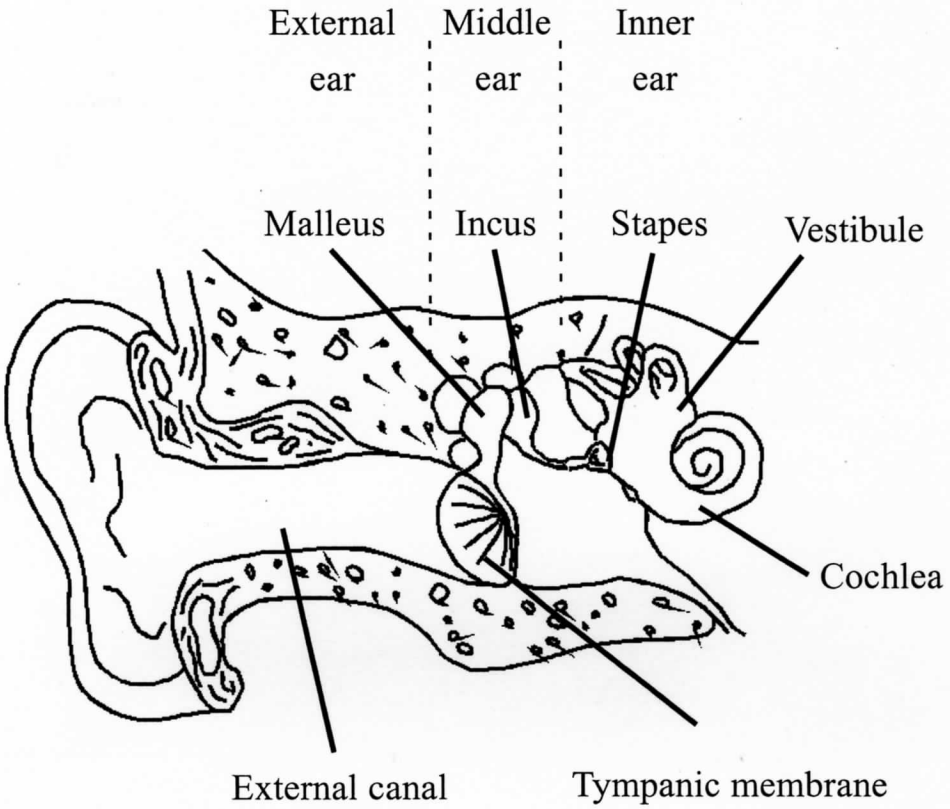

Figure 1.1. Schema of human auditory system. The auditory system is divided into external ear, middle ear and inner ear. The sound entering the external auditory canal vibrates the tympanic membrane. This vibration is mechanically transmitted by the ossicles (malleus, incus and stapes) to the cochlea.

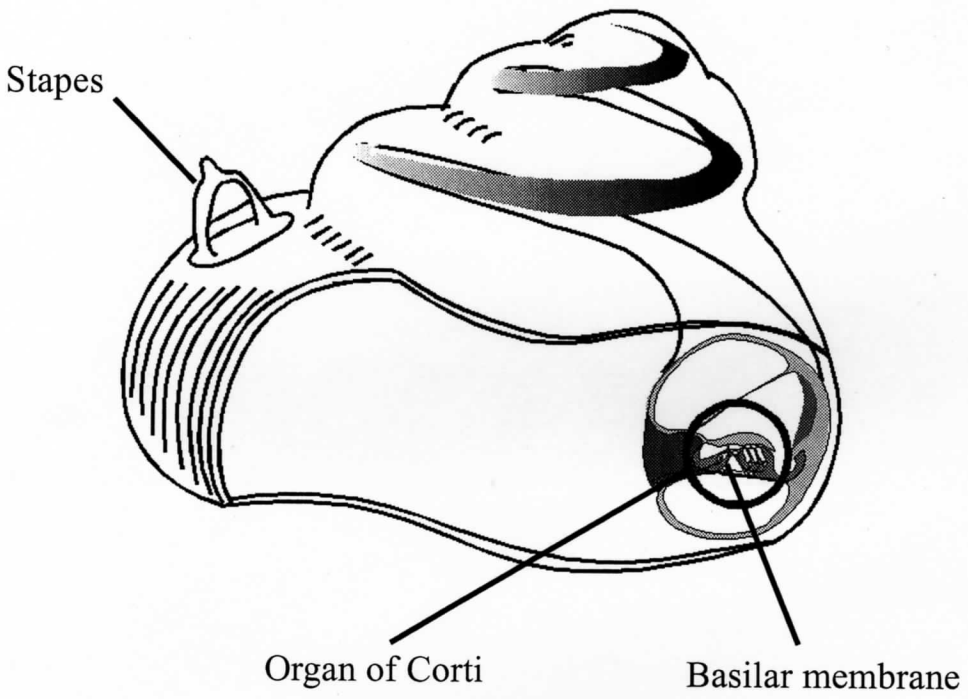

Figure 1.2. Outline of the cochlea of human. The cochlea has spiral shape which is filled with fluid. When the stapes delivers vibrations from the middle ear to the fluid-filled cochlea, due to the change in the fluid pressure, the travelling wave occur to the basilar membrane. The basilar membrane supports the sensory organ of hearing, i.e., the organ of Corti.

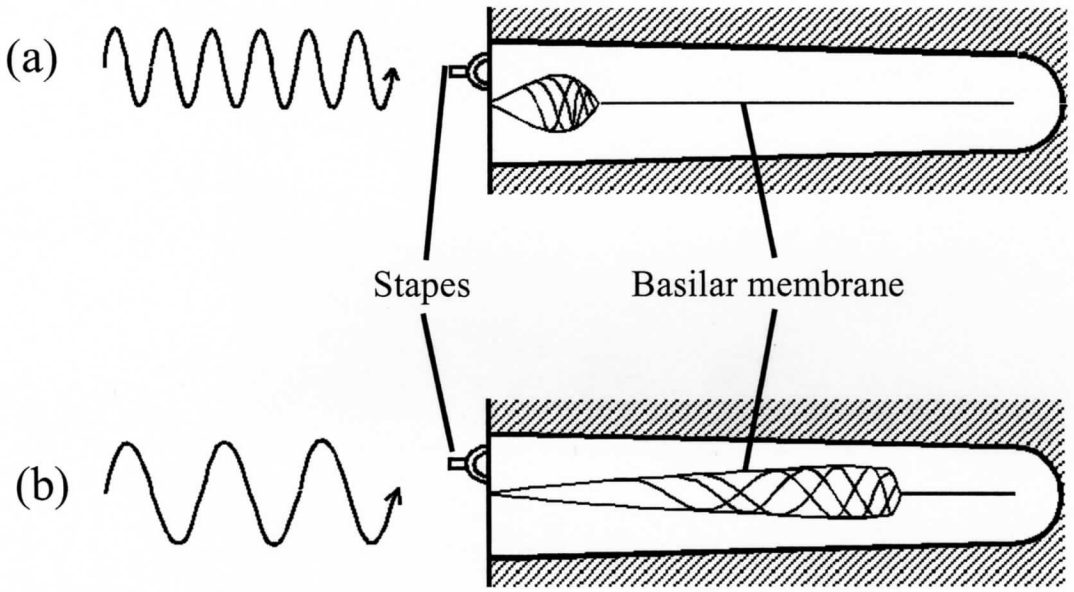

Figure 1.3. Traveling waves on the basilar membrane. Vibrations of the stapes generate movement of the cochlear fluids, which interact with the stiffness of the basilar membrane (BM), and produce progressive traveling wave on the BM. (a) The traveling waves on the BM have a peak near the base when high frequency sounds enter the cochlear. (b) The low frequency sounds develop the traveling waves on the BM which has a peak near the apex.

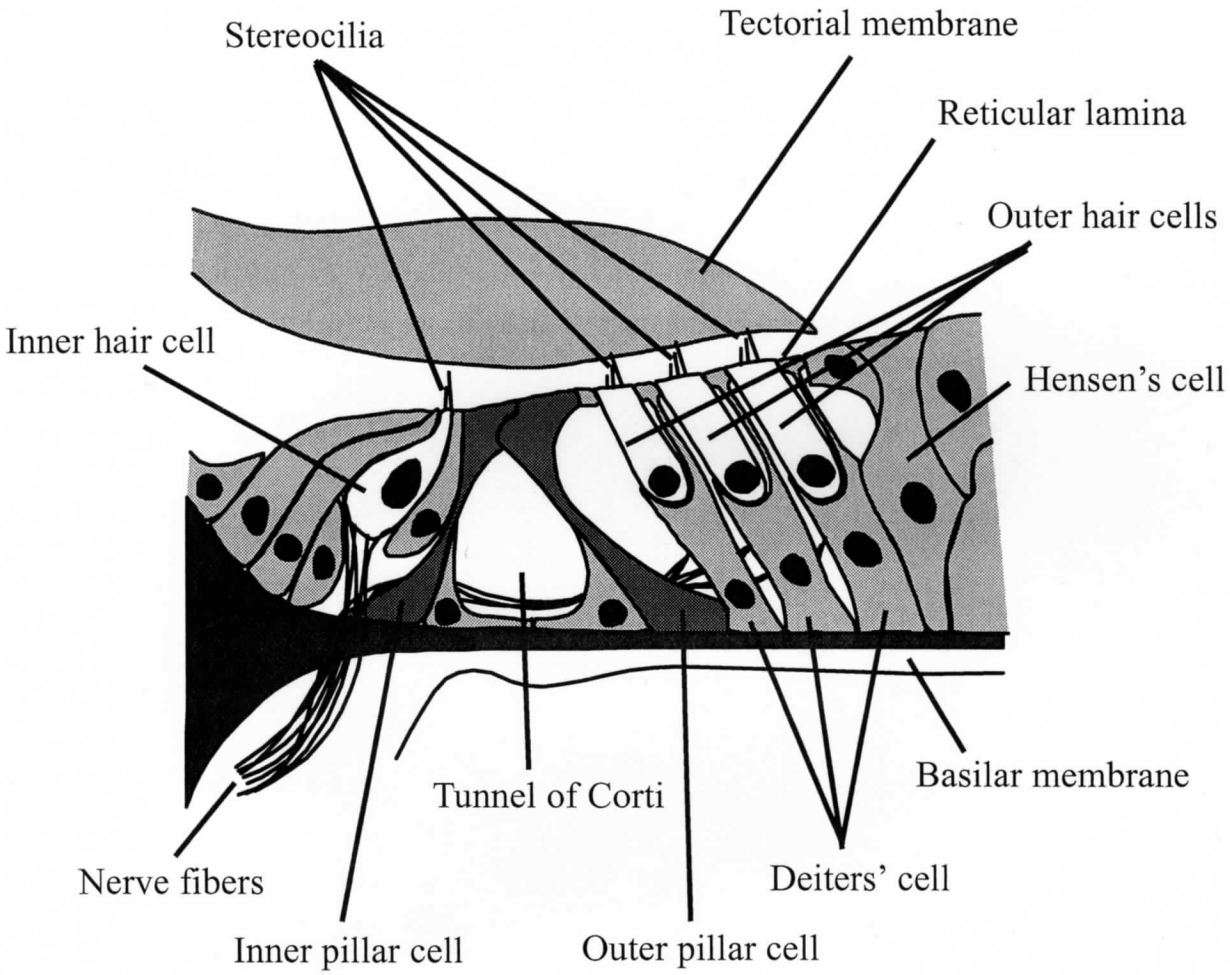

Figure 1.4. Structure of the organ of Corti. The organ of Corti sits on the basilar membrane, and it contains an array of supporting cells, outer hair cells and inner hair cells. Tectorial membrane is above the organ of Corti.

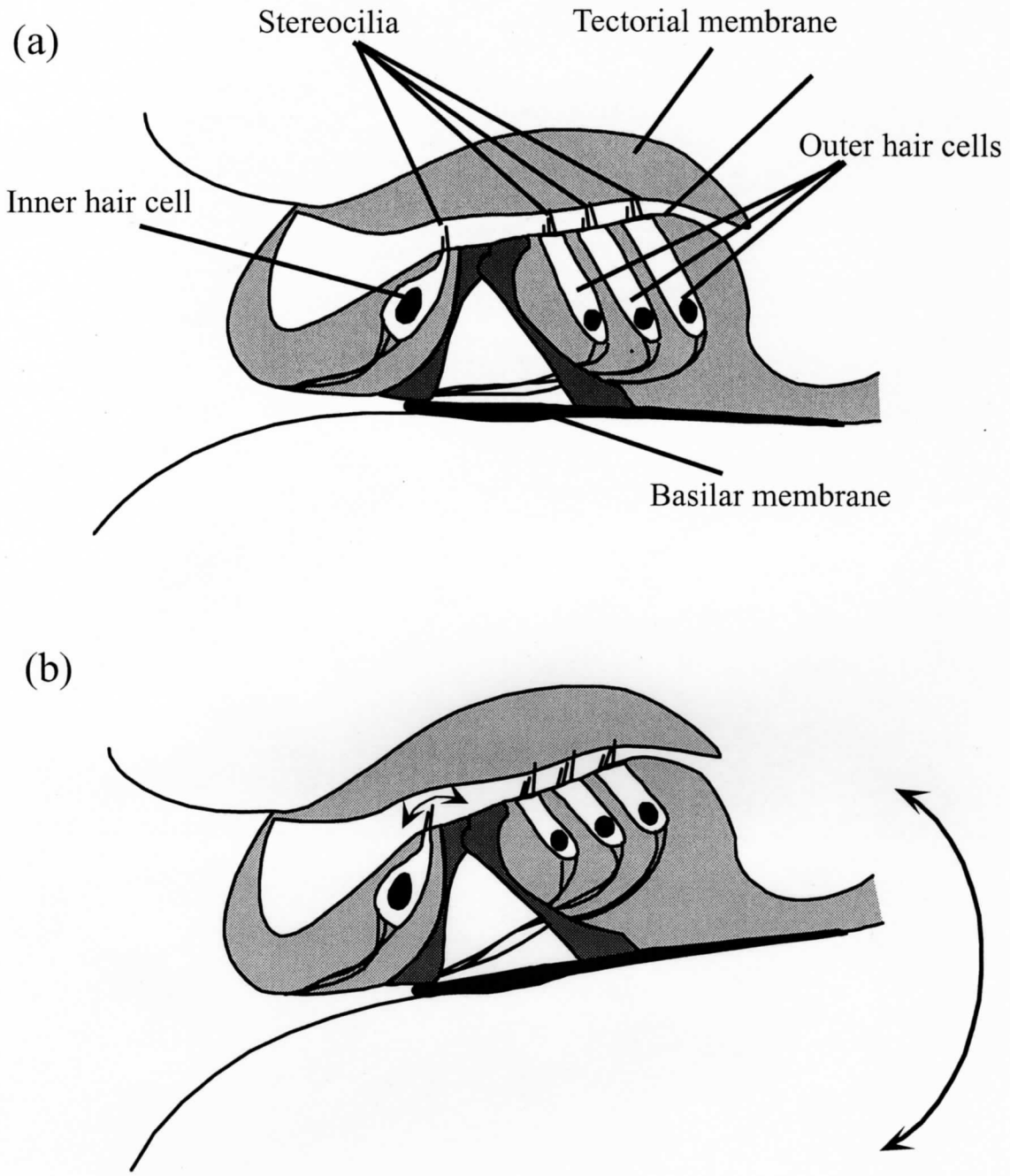

Figure 1.5. Mechanism of the transduction in the organ of Corti. (a) Resting state of the organ of Corti. (b) Bending motion of the organ of Corti. When the sound enter the ear, the organ of Corti has a bending motion. This bending motion generates the movement of the fluids in the space between the undersurface of the tectorial membrane and the reticular lamina, which leads to the deflection of the stereocilia of the IHCs. By this deflection, the potential in the IHCs is changed and the transmitter is released. As a result, action potential are produced in the auditory nerve fiber.

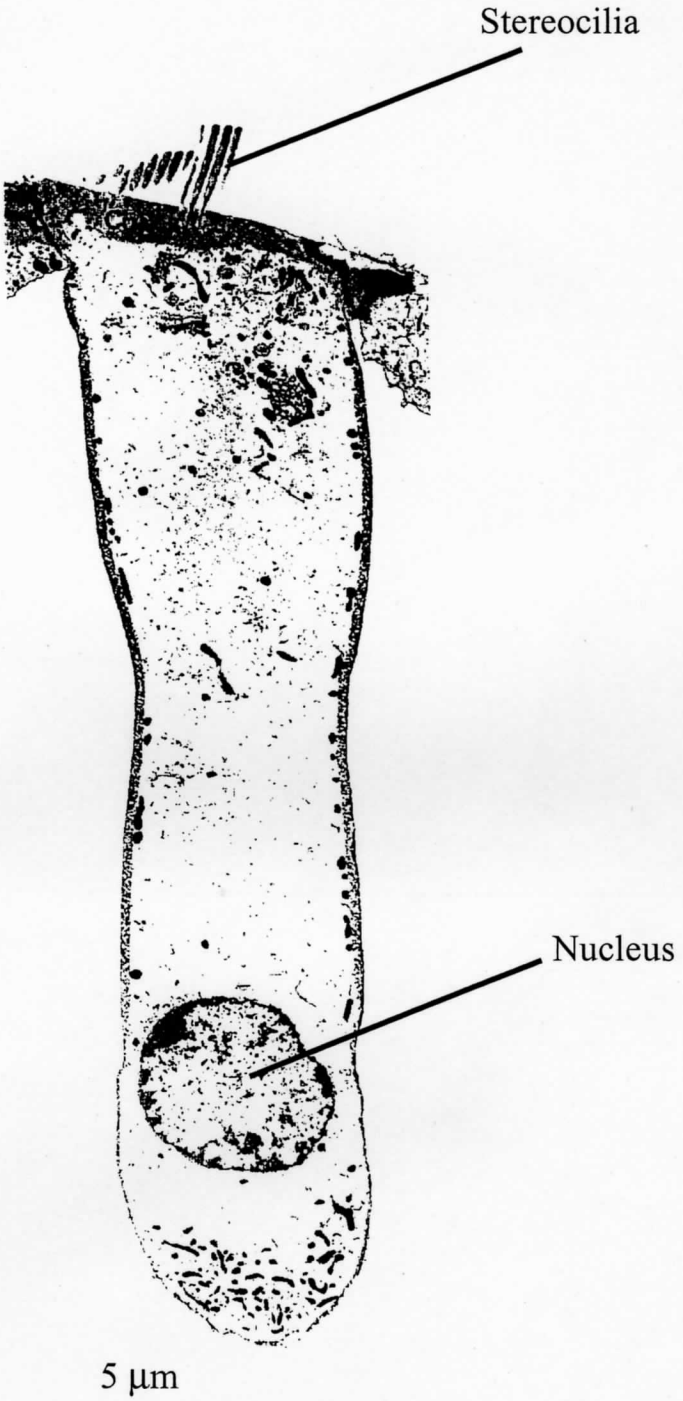

Figure 1.6. Longitudinal section of the outer hair cell which is observed using transmission electron microscope (Saito, 1983). Outer hair cell is characteristically cylindrical in shape with a hair bundle, stereocilia, at its apical end and a nucleus near its base. It varies in length from 30 μm to 90 μm, and it has a regular diameter of 10 μm.

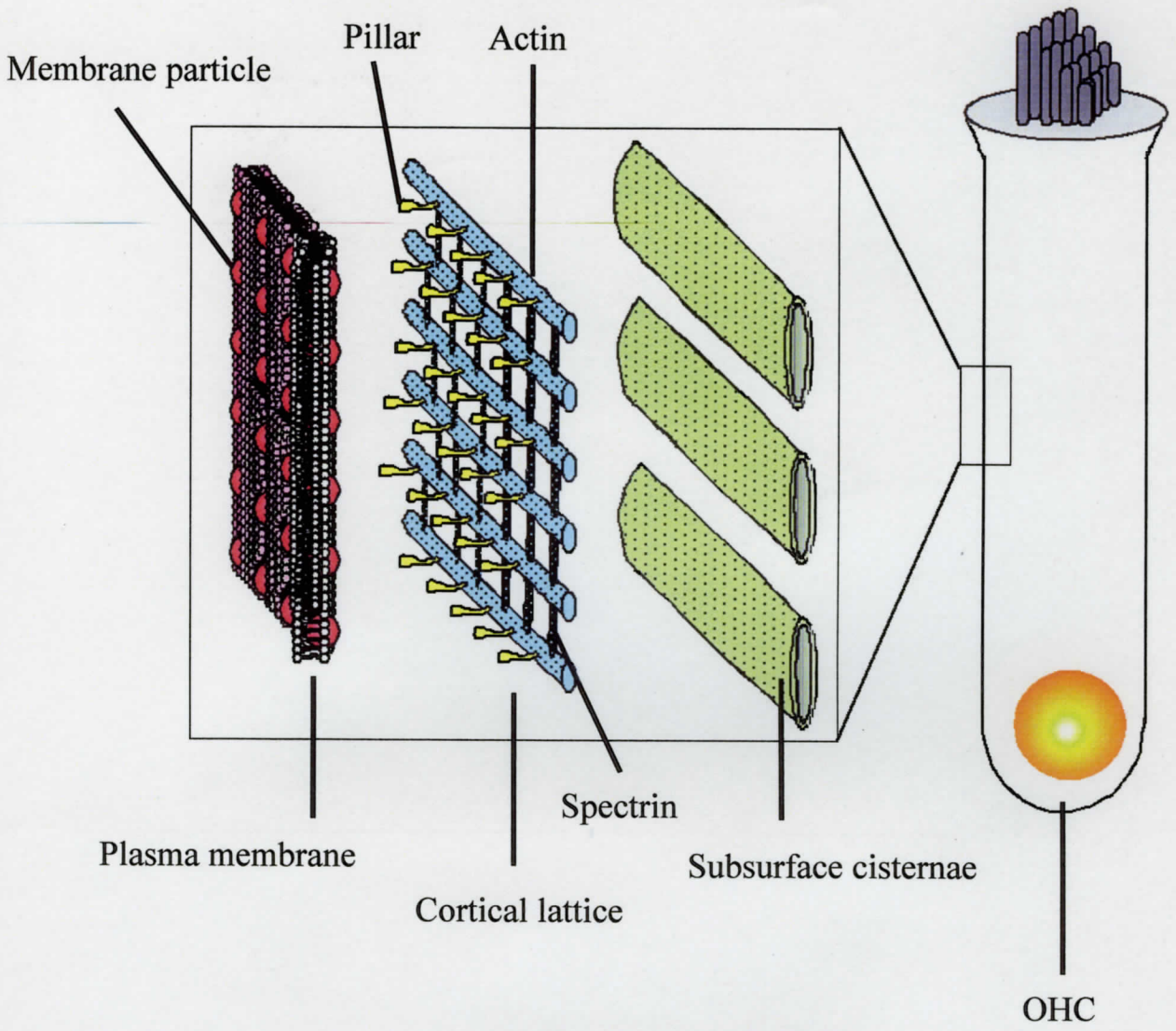

Fig. 1.7. Lateral wall of the OHC. The OHC lateral wall consists of three layers: plasma membrane, cortical lattice and subsurface cisternae. The cortical lattice is located between the subsurface cisternae and the plasma membrane, and it consists of two types of filaments: actin and spectrin. Actins, which are arranged circumferentially, are 5-8 nm in diameter and are cross-linked at regular intervals by thinner spectrins, 2-4 nm in diameter. The outermost plasma membrane is linked to the cortical lattice by the pillars and contains a high density of membrane particles. The innermost subsurface cisternae are known to be much more fluid than the plasma membrane.

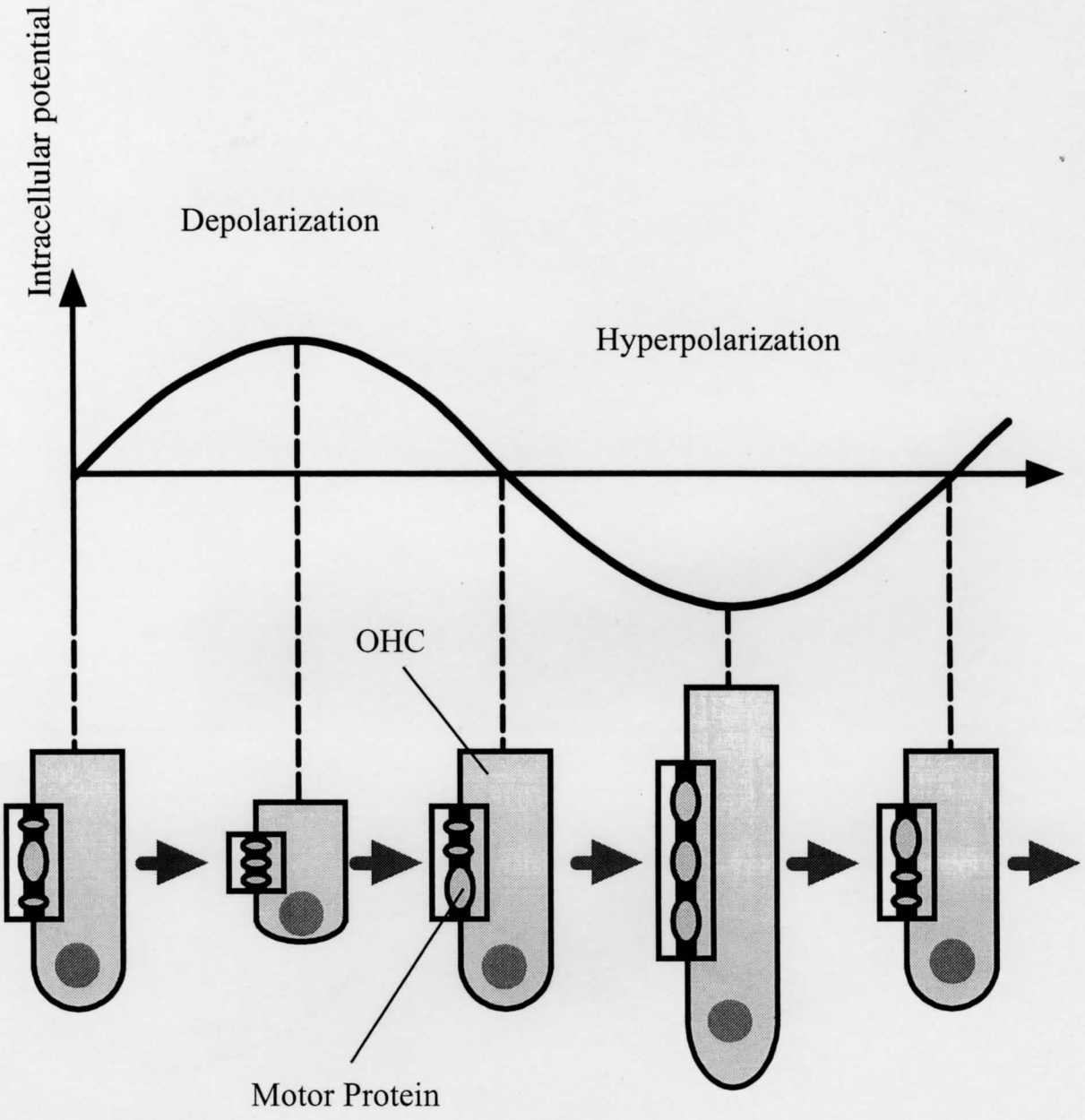

Figure 1.8. OHC electromotility. As the stereocilia has the ion channel, the intracellular potential is depolarized and hyperpolarized while the stereocilia is bending *in vivo*. When the intracellular potential is depolarized, the OHC contracts. On the other hand, the OHC elongates when the intracellular potential is hyperpolarized. This OHC motility is thought to be associated with the conformational changes of the membrane particles, which are called "motor protein."

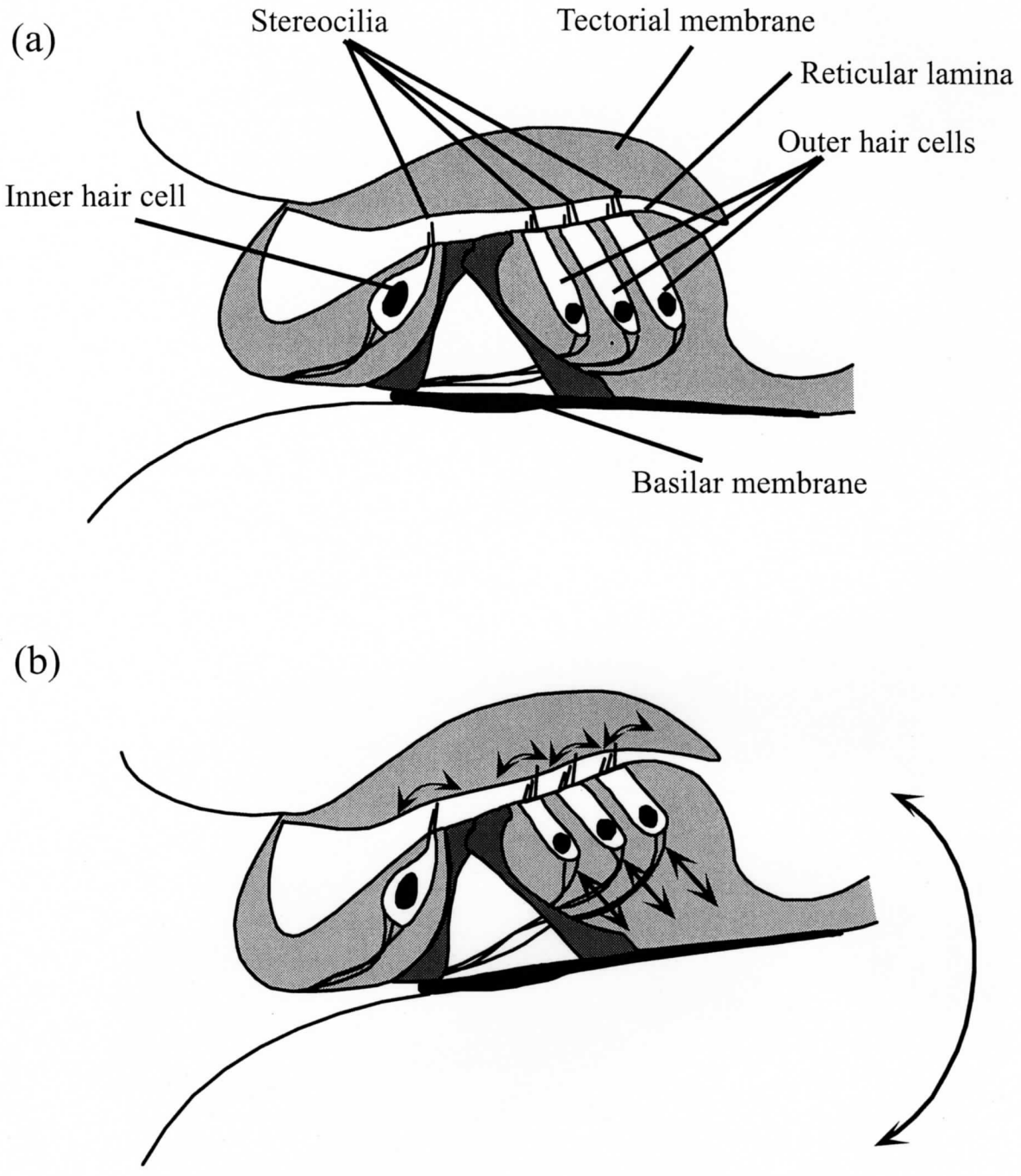

Fig. 1.9. Cochlear amplification. (a) Resting state of the organ of Corti. (b) Bending motion of the organ of Corti. When the organ of Corti undergoes a bending motion, the stereocilia of the OHCs bend due to the shear motion between the tectorial membrane and the reticular lamina. This bending of the stereocilia induces the OHCs motility. As the force produced by the OHCs motility magnifies the deflection of the organ of Corti, the movement of the fluids in the space near the stereocilia of the IHCs and the deflection of the IHC stereocilia increases.

2. Materials and methods

2.1. Local deformation of the OHC

2.1.1. Cell preparation

Guinea pigs (200-300g) were decapitated and the temporal bones were removed. After opening the bulla, the cochlea was detached and transferred to the experimental bath (the major ions in the medium are: NaCl, 140mM; KCl, 5mM; $CaCl_2$, 1.5mM; $MgCl_2 \cdot 6H_2O$, 1.5mM; HEPES, 5mM; Glucose, 5mM; pH 7.2; 300mOsm). The bony shell covering the cochlea was removed and the middle two turns of the organ of Corti were gently scraped off from the basilar membrane. After enzymatic incubation with dispase (500PU/ml), the OHCs were isolated by pipetting gently the organ of Corti in the experimental bath . The isolated OHCs were transferred to a chamber, and the medium, which contained microspheres 0.75μm in diameter, was perfused from the pipette. Under these procedures, the microspheres were randomly attached to each cell. All experiments were performed at a room temperature.

2.1.2. Hypotonic stimulation

The OHCs were perfused with the hypotonic solution (H_2O; 0mOsm) through the pipette having tip sizes of 10-20μm. As the osmotic pressure of the hypotonic solution was lower than the intracellular osmotic pressure of the OHC, the osmotic water was transported across the cells membrane. As a result, the intracellular pressure was increased, and the cell shape change was evoked. The images of the cell were stored with a CCD camera system (C2400, HAMAMATSU).

2.1.3. Electrical stimulation

The OHCs were whole-cell voltage clamped, using an Axon 200B amplifier with patch pipettes having initial resistances of 3-5 MΩ, corresponding to tip sizes of 1-2μm (Hamill et al., 1981). The patch pipette solution was composed of 150mM KCl, 2mM $MgCl_2 \cdot 6H_2O$, 10mM EGTA and 10mM HEPES buffered to pH7.2. A sinusoidal command voltage of 120mV in amplitude and 5Hz in frequency, was applied to the cell. The images of the cell were stored with a high speed video system (HSV-500DM, nac). The record rate of this system was 250 frames per second which was about eight times faster than that of the conventional video system with 30 frames per second.

2.1.4. Data analysis

In this study, every images were analyzed off-line using a personal computer. One pixel in the recorded digital picture from the CCD camera system corresponded to 210nm, and that from the high speed video system was equal to 150nm. Each pixel was quantified to 256 grayscales. For the purpose of analyzing a microsphere displacement smaller than 1 pixel, a high-resolution motion detection method was applied (Fig. 2.1). Quantification of the movement was done on the digitized images by placing a measuring rectangle arbitrary aligned across the microsphere on the cell lateral wall (Fig. 2.1(a)). At an arbitrary time slice, changes in the brightness alined along the measuring rectangle were fitted by a cubic regression line, and the peak of the fitted line was determined to be the position of the microsphere (Fig. 2.1(b)). At another time slice, a cubic regression line was also obtained, and the displacement of the microsphere was calculated from the shift in the peak of the fitted lines (Fig. 2.1(b)).

In this analysis, the noise in the recorded digital picture and Brownian motion of the microsphere caused the analytical error. Therefore, the analytical error was

evaluated by measuring the position of the fixed microsphere at some time slices without the perfusion nor the electrical stimulation. The time histories of the position of the fixed microsphere in the recorded digital picture from the CCD camera system are depicted in Fig. 2.2, and the figure shows that the position of the fixed microsphere at every time slices varies. Therefore, the maximum difference of the position in Fig. 2.2 was decided to be the value of the analytical error in the recorded digital picture from the CCD camera system and it corresponded to 170nm. In the same way, the value of the analytical error in the recorded digital picture from the high speed video system was evaluated and corresponded to 120nm.

2.2. Ultrastructure of the OHC

2.2.1. Cell preparation

The OHCs were isolated from apical and middle two turns of the organ of Corti in the same way as shown in section 2.1.1. The isolated OHCs were transferred to a chamber and fixed in the 2.5% glutaraldehyde in phosphate buffer for 30 min at room temperature. After fixation, the OHCs were washed with an experimental bath.

2.2.2. Atomic force microscopy

Images of the OHC lateral wall were recorded in the experimental bath with an AFM (NVB100, OLYMPUS). The AFM was mounted on an inverted microscope. V-shaped silicon nitride cantilevers and pyramidal tips (OMCL-TR400PSA-2, OLYMPUS) were used. The spring constant of the cantilever was 0.08 N/m and tip's typical radius of curvature was less than 20 nm. In this experiment, tapping mode under the fluid was used. In the tapping mode, the tip was oscillated with high

frequency in the vertical direction and was only intermittently in contact with sample. The images obtained by the measurement from the AFM were analyzed by the software provided by Digital Instruments. In order to reduce the noise and correct for tilt, the images were flatten and plane fit. The features of the images were evaluated by the section analysis. In this analysis, the images were sectioned to learn about their surface profiles and the size or distance of the surface features were measured.

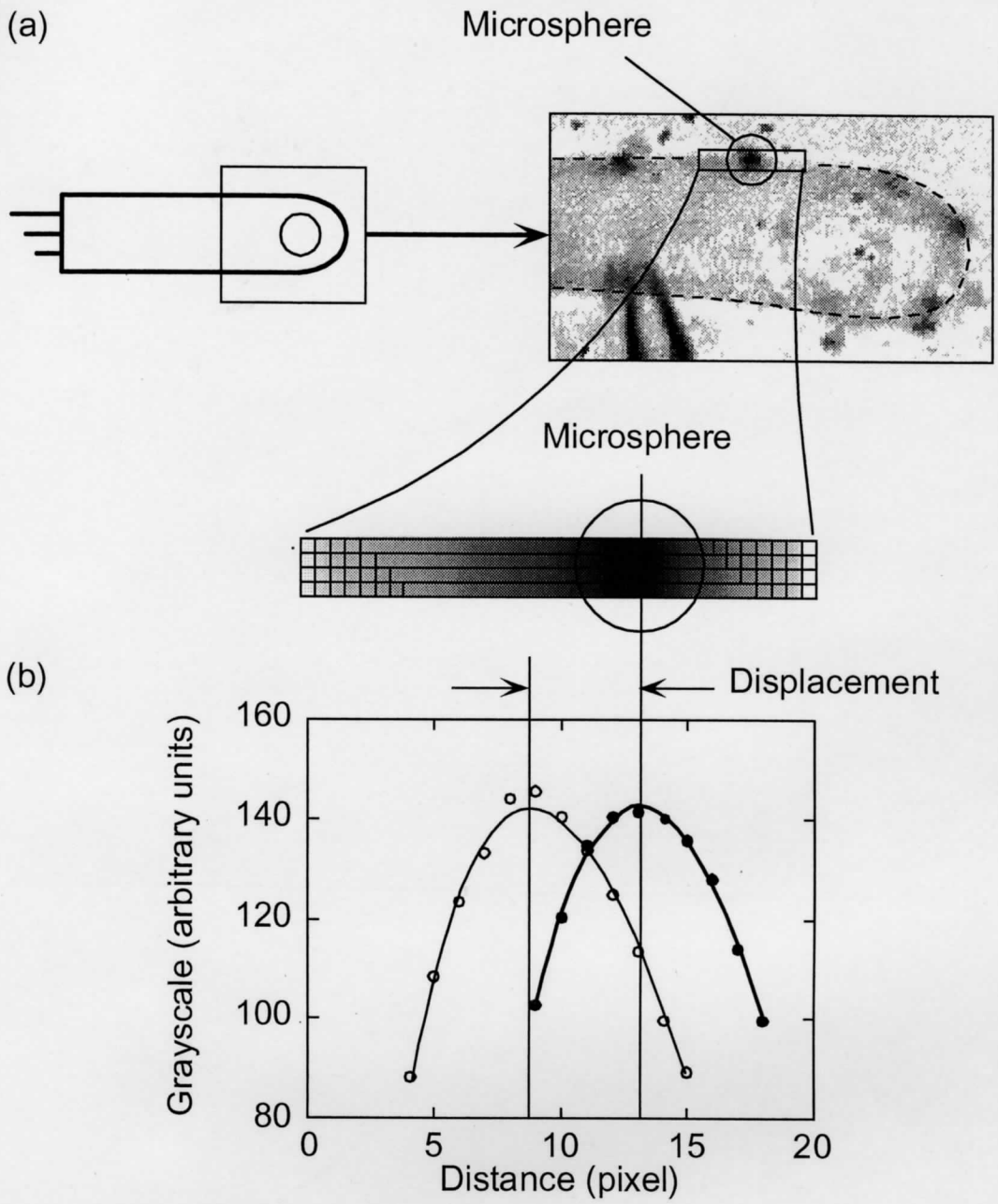

Fig. 2.1. Quantification of microsphere displacement. (a) Basal part of an OHC at an arbitrary time slice. A measuring rectangle arbitrarily aligned across the microsphere is shown, and it composes of 4 rows of pixels. (b) Changes in brightness along the measuring rectangle. The mean brightness is calculated for each vertical column of the pixels inside the measuring rectangle, and plotted by a solid circle. The solid circles obtained by a repetition of this procedure are fitted by a cubic regression line and its peak is determined to be a position of the microsphere at an arbitrary time slice. Next, at another time slice, the mean brightness is calculated in the same way and shown by the open circles. They are also fitted by a cubic regression line and its peak is determined to be a position of the microshere at another time slice. Finally, the distance between the two peaks is quantified to be the microsphere displacement.

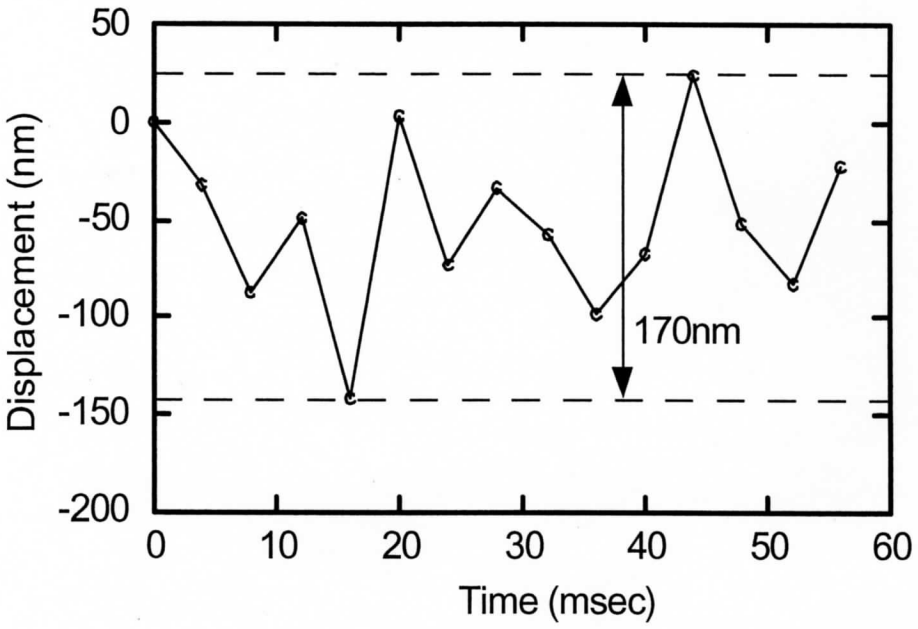

Fig. 2.2. Time histories of the position of the fixed microsphere in the recorded digital picture from a CCD camera system without the perfusion nor the electrical stimulation. The position of the fixed microsphere at some time slices varies because of the analytical error which is caused by the noise in the recorded digital picture and Brownian motion of the microsphere. The value of the analytical error is calculated from the maximum difference of the position and corresponds to 170nm.

3. Results

3.1. Local deformation of the OHC

3.1.1. Cell shape changes evoked by the hypotonic stimulation

When the OHCs were perfused with the hypotonic solution, the cell shape changes were evoked and the cylindrically shaped OHCs showed large longitudinal shortening and small circumferential extension. As the longitudinal stiffness was concerned with the electromotility, the longitudinal displacement values of the several points on the cell were measured. The measurement points on one of the cells are shown in Fig. 3.1(a), and the longitudinal displacement values of the measurement points at 5% shortening of the cell length are depicted in Fig. 3.1(b). The abscissa represents the distance of each measurement point from the basal end of the cell, and the positions of the basal and apical ends along the cell axis are converted to 0.0 and 1.0, respectively. The ordinate represents the displacement values of the measurement points. As the direction of the arrow in Fig. 3.1(a) represents the positive of the displacement, it is clear that the displacement value at the center part of the cell is zero and the basal and apical parts move toward the center of the cell. Besides, it is obvious that the displacement values are almost constant to be -1.36μm (displacement at the apical end) in the region near the apical end, and they vary linearly in the other region. In order to correlate the displacement values with the distance along the cell axis in detail, an attempt is made to obtain a regression line. First, the measurement points of the apical end and the microsphere 2 which has nearly the same displacement value as that of the apical end within the analytical error (170nm) are deleted. Then, the displacement values of the remained measurement points are fitted by a linear regression line (Fig. 3.2(a)). It has a slope of -5.36 and the correlation coefficient r of 0.992, and the displacement value obtained from the regression line is equal to that of the apical end (-1.36μm) at the point 0.851 from the basal end. Figure 3.2(a)

shows that the displacement values are proportional to the distance along the cell axis in the region between 0.0 and 0.851 from the basal end and that the displacement values are constant to be -1.36μm in the region between 0.851 and 1.0 from the basal end. This result indicates that the local deformation is constant in the region between 0.0 and 0.851 from the basal end and does not occur in the region between 0.851 and 1.0 from the basal end (Fig. 3.2(b)).

In the same way as shown in Fig. 3.1, the data from the 10 different cells are analyzed. Fig. 3.3(a) shows the 10 regression lines obtained from the cells. Each correlation coefficient r is between 0.982 and 0.997. The OHC lengths used in this analysis ranged from 53.92μm to 80.67μm. In order to show the data obtained from the different cells, the displacement values of the ordinate are normalized by converting those of the basal end to 1.0 and those of the apical end to 0.0. The regression lines cross the displacement 0 line (dotted line in Fig. 3.3(a)) at the point 0.881±0.0447 (mean±standard deviations) from the basal end. This result shows that the displacement values are proportional to the distance along the cell axis in the region between 0.0 and 0.881±0.0447 from the basal end and that the displacement values are constant to be 0.0 in the region between 0.881±0.0447 and 1.0 from the basal end. The outcome indicates that the local deformation is almost constant in the region between 0.0 and 0.881±0.0447 from the basal end and it does not occur in the region between 0.881±0.0447 and 1.0 from the basal end (Fig. 3.3(b)).

3.1.2. Cell shape changes evoked by the electrical stimulation

A 5.0Hz sinusoidal command voltage was applied to the OHC. The measurement points on one of the cells are shown in Fig. 3.4(a), and the time histories of the measurement points are depicted in Fig. 3.4(b). As the direction of the arrow in Fig. 3.4(a) represents the positive of the displacement, Fig. 3.4(b) shows that the cell has

a maximum contraction at 50 msec and a maximum elongation at 150 msec. The displacements of the measurement points at the maximum contraction are shown in Fig. 3.5(b). The abscissa represents the distance of each measurement point from the basal end of the cell, and the positions of the basal and apical ends along the cell axis are converted to 0.0 and 1.0, respectively. The results show that the displacement values are almost constant to be 3.53μm (displacement at the basal end) and -4.18μm (displacement at the apical end) in the regions near the basal and apical ends, respectively. By contrast, in the middle region of the cell, the displacement values vary almost linearly. In order to correlate the displacement values with the distance along the cell axis in detail, an attempt is made to obtain a regression line in the same way as shown in section 3.1.1. First, the measurement points of the apical end and the basal end and the microspheres 2 and 9 which have nearly the same displacement value as that of the basal or apical end within the analytical error (120nm) are deleted. Then, the displacement values of the remained measurement points, which are in the middle region of the cell, are fitted by a linear regression line (Fig. 3.6(a)). It has a slope of -11.1 and the correlation coefficient r of 0.995 and the displacement values obtained from the regression line are equal to that of the basal end (3.53μm) at the point 0.160 and that of the apical end (-4.18μm) at the point 0.855 from the basal end. Fig. 3.6(a) shows that the displacement values are proportional to the distance along the cell axis in the region between 0.160 and 0.855 from the basal end and that the displacement values are constant to be 3.53μm and -4.18μm in the regions between 0.0 and 0.160 and between 0.855 and 1.0 from the basal end, respectively. This result indicates that the local deformation in the middle region of the cell is constant and the local deformation does not occur in the regions between 0.0 and 0.160 and between 0.855 and 1.0 from the basal end (Fig. 3.6(b)).

In the same way as shown in Fig. 4, the data from the 10 different cells are

analyzed. Fig. 3.7(a) shows the 10 regression lines obtained from the cells. Each correlation coefficient r is between 0.936 and 0.995. The OHC lengths used in this figure ranged from 47.10μm to 59.10μm. In order to show the data obtained from the different cells, the displacement values of the ordinate are normalized by converting those of the basal end to 1.0 and those of the apical end to 0.0. The regression lines cross the displacement 1.0 line at the point 0.142±0.0705 (mean±standard deviations) and the displacement 1.0 line at the point 0.893±0.0491 from the basal end. This result shows that the displacement values are proportional to the distance along the cell axis in the region between 0.142±0.0705 and 0.893±0.0491 from the basal end, and that the displacement values are constant to be 1.0 in the region between 0.0 and 0.142±0.0705 and 0.0 in the region between 0.893±0.0491 and 1.0 from the basal end. The outcome indicates that the local deformation in the middle region of the cell is constant and the local deformation does not occur in the regions between 0.0 and 0.142±0.0705 and between 0.893±0.0491 and 1.0 from the basal end (Fig. 3.7(b)).

3.2. Ultrastructure of the OHC lateral wall

3.2.1. Tip-sample interaction

The oscillating tip was approached to the OHC surface which was fixed in the 2.5% glutaraldehyde in phosphate buffer for 30 min. The tip-sample approach curve is shown in Fig. 3.8. The center of the tip oscillation and the amplitude of the oscillating tip were plotted against the cantilever position. The red line indicates the curve when the cantilever approached to the OHC surface and the blue line indicates the curve when the cantilever withdrew from the OHC surface. When the oscillating tip was approached to the OHC surface, the amplitude of the oscillating tip decreased

by slow degrees in the region between A and B. It is considered that this phenomenon is caused from the viscous resistance of the liquid between the tip and the OHC surface. In the region between B and C, the amplitude of the oscillating tip decreased and the center of the oscillation shifted upward. This indicates that the tip is contact with the OHC surface and the tip-sample interaction in this region is suited to scanning. Therefore, the set point amplitude (the set point voltage) was set in this region.

3.2.2. Circumferential filaments

The lateral surface of the fixed OHC was scanned using the AFM tapping mode. Figure 3.9 shows the image which was obtained in the apical region of the OHC. The position of the scanning area is shown in Fig. 3.9(a), and the image is shown in Fig. 3.9(b). The scanning area was 1 μm × 2 μm. From this image, the filaments which are arranged circumferentially were discerned. Figure 3.10 shows the image which was obtained in the middle region of the OHC. The scanning area was 1 μm × 2 μm and this image was obtained with a scan angle which was different from Fig. 3.9. From this image, the filaments which are arranged circumferentially were also discerned. These filaments could be seen in the images which were obtained in every region of the OHC and all of them were arranged circumferentially. In order to evaluate the circumferential filaments, the intervals of the circumferential filaments were measured by the section analysis. In this analysis, the 0.5 μm × 1 μm scan area image was sectioned along the line which is orthogonal to the direction of the filaments and the surface profile of the section was plotted (Fig.3.11(b)). From this surface profile, the intervals of the circumferential filaments were measured. Using this analysis, the intervals of the circumferential filaments were measured from the 38 images which were scanned in the region between 0.1 and 0.98 from the basal end. Figure 3.12 shows the number of measurements which is plotted against the

interval in 10 nm classes. The intervals are ranged from 15 nm to 103 nm and the mean and the standard deviation of them were 49 nm and 18 nm, respectively.

(a)

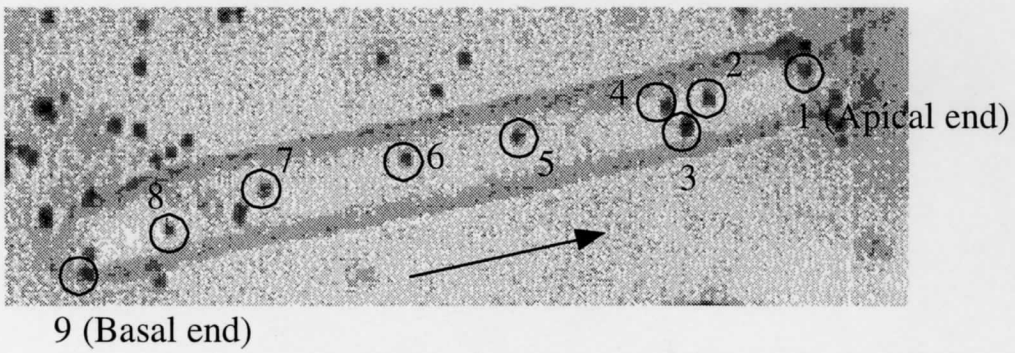

(b)

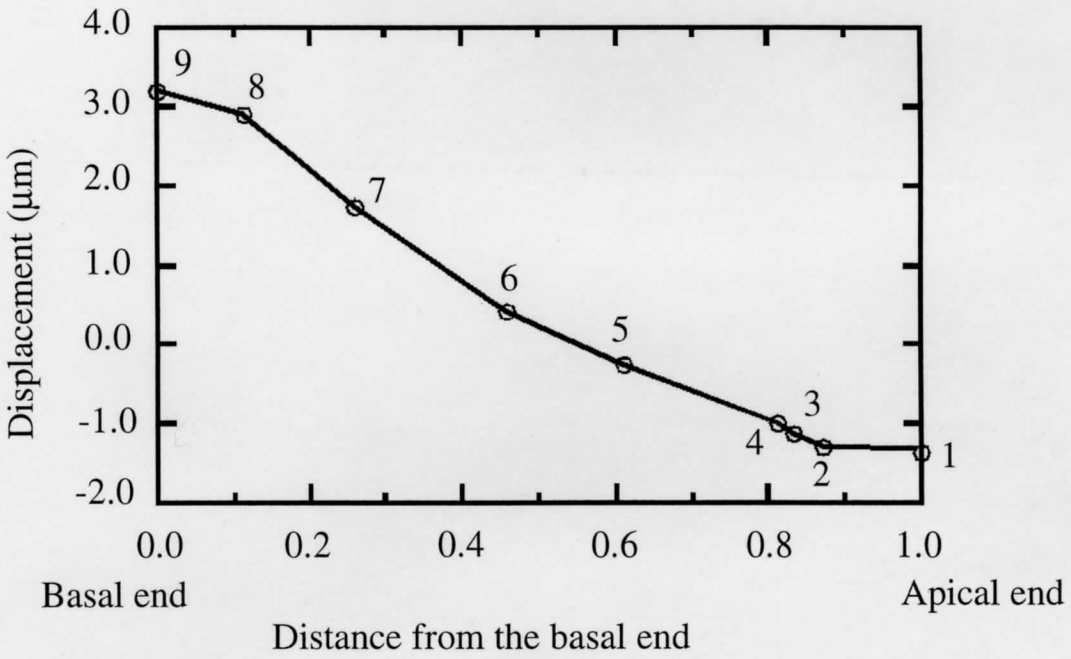

Fig. 3.1. The axial displacement values of the microspheres attached to the lateral wall of the cell with hypotonic solution perfusion. (a) Measurement points on the cell. Black points marked by the open circles are the measurement points. The measurement points of microspheres 1 and 9 correspond to those of the apical and basal ends. (b) The axial displacement values of the measurement points shown in (a).

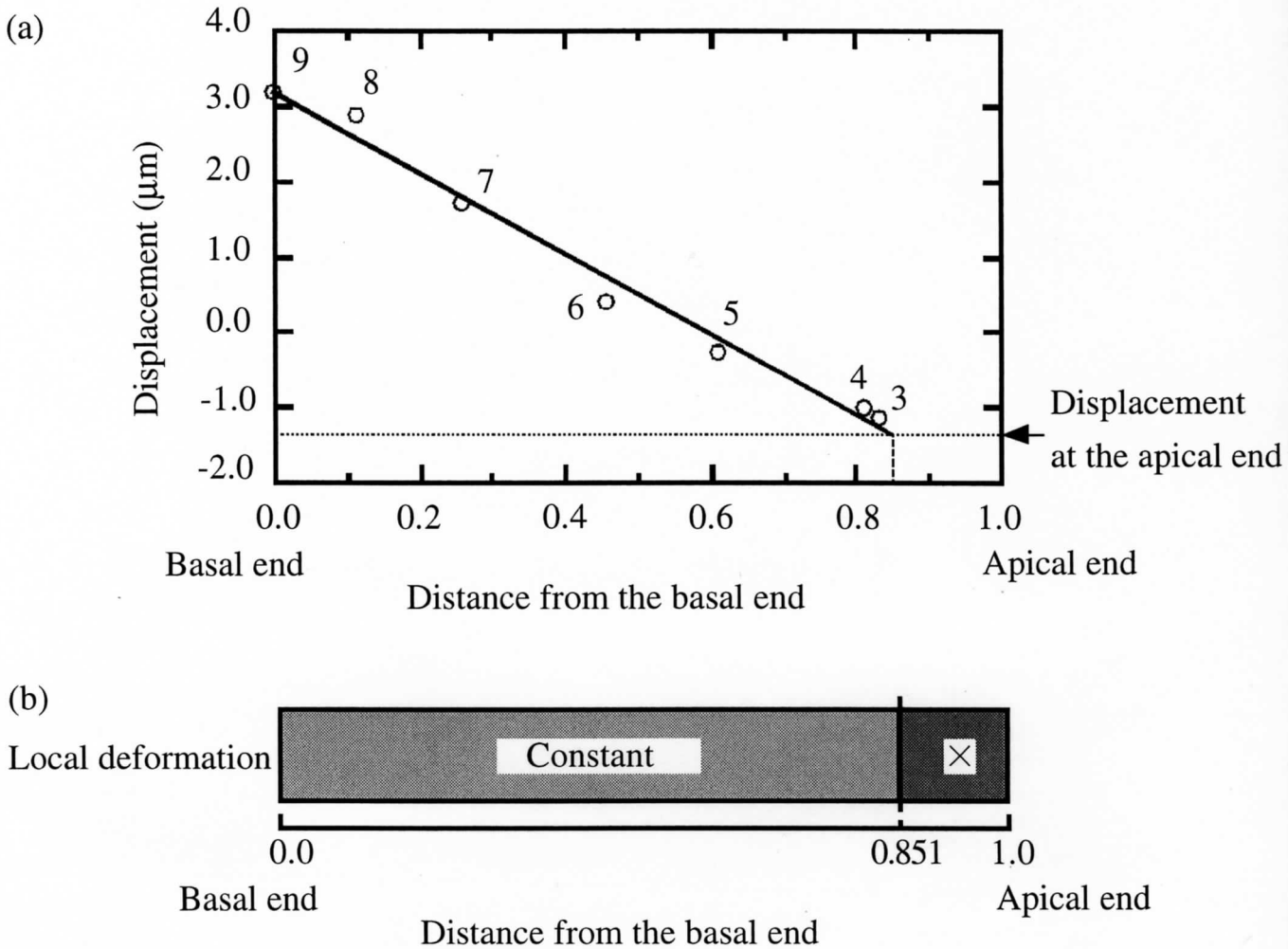

Fig. 3.2. Evaluation of the correlation between the displacement values and the distance along the cell axis. (a) The axial displacement values of the measurement points except those of the apical region of the cell. The solid line is a linear regression line given by $y = 3.20-5.35x$; $r = 0.992$. The displacement value obtained from the regression line is equal to that of the apical end (-1.36 μm) at a point 0.851 from the basal end. This figure shows that the displacement values are proportional to the distance along the cell axis in the region between 0.0 and 0.851 from the basal end and that the displacement values are constant in the region between 0.851 and 1.0 from the basal end. (b) The local deformation of the cell. This figure shows that the local deformation is almost constant in the region between 0.0 and 0.851 from the basal end and that it does not occur in the region between 0.851 and 1.0 from the basal end.

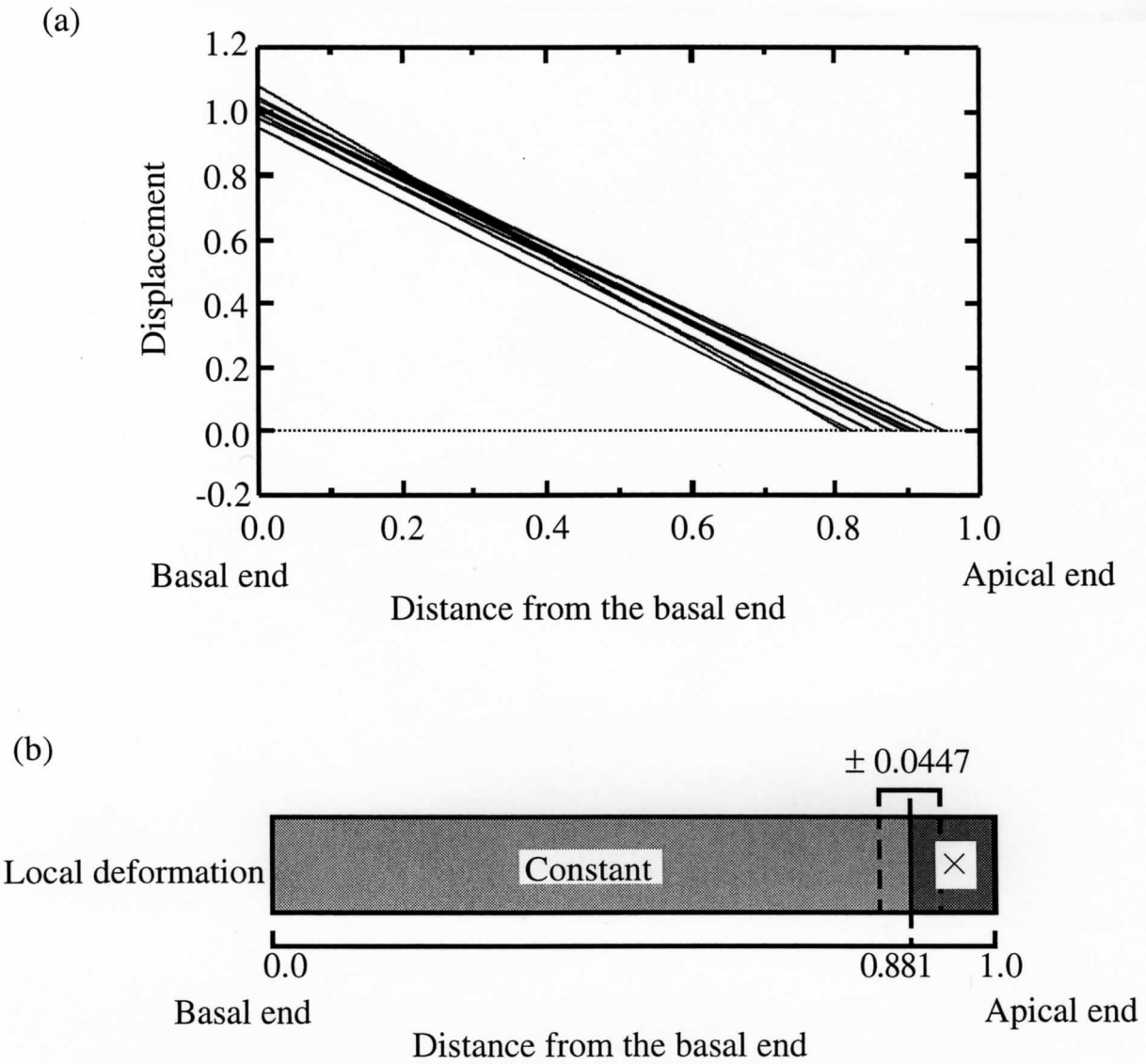

Fig. 3.3. The local deformation evoked by the hypotonic stimulation. (a) Normalized axial displacements of the measurement points except in the apical region of the cell. The solid line shows the 10 linear regression lines obtained from the 10 different cells. (b) The local deformation of the cell. Figure. 4.3(a) shows that the displacement values are proportional to the distance along the cell axis in the region between 0.0 and 0.881 ± 0.0447 (mean ± standard deviations) from the basal end and that the displacement values are constant in the region between 0.881 ± 0.0447 and 1.0 from the basal end. Figure. 4.3(b) shows that the local deformation is almost constant in the region between 0.0 and 0.881 ± 0.0447 from the basal end and it does not occur in the region between 0.881 ± 0.0447 and 1.0 from the basal end.

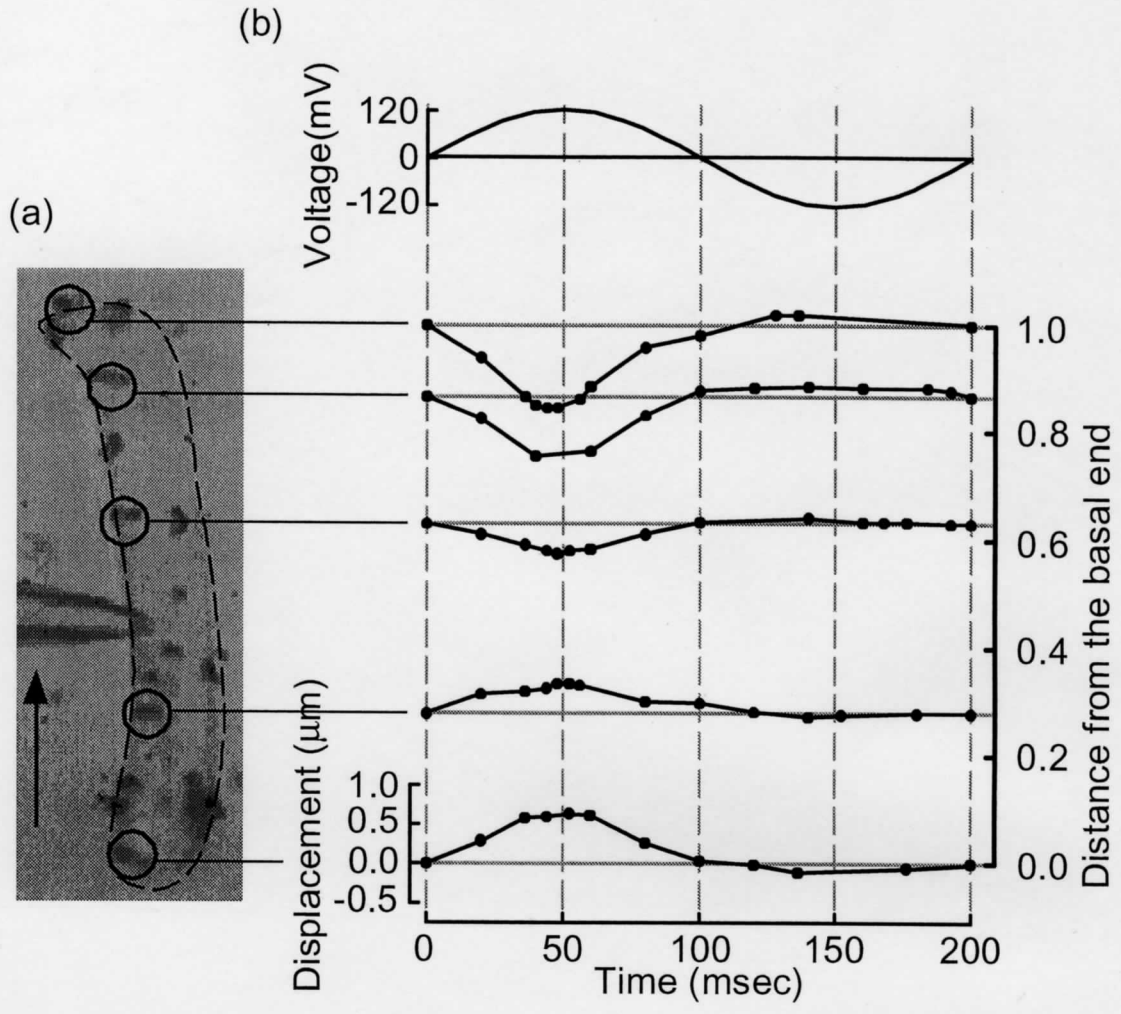

Fig. 3.4. Axial displacements of the microsphere attached to the cell lateral wall when a 5.0Hz sinusoidal command voltage was applied. (a) Measurement points on the cell. Black points marked by the open circles are measurement points. (b) Time histories of the axial displacement of the measurement points shown in (a). The top trace shows the 5.0Hz sinusoidal command voltage which was applied to the OHC.

(a)

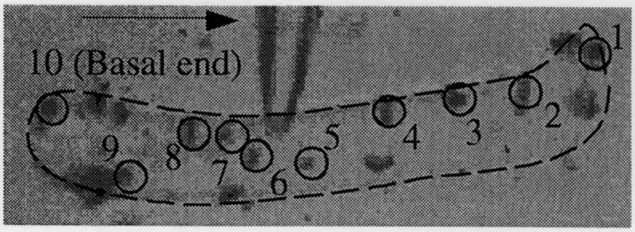

(b)

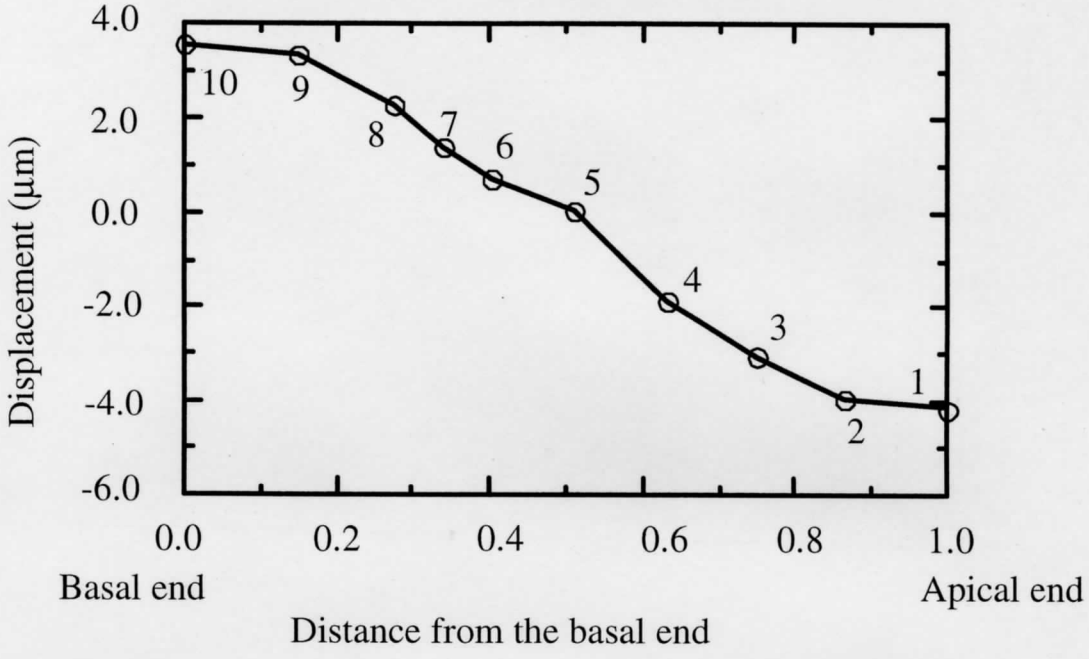

Fig. 3.5. Axial displacements of the microsphere attached to the cell lateral wall at the maximum contraction when a 5.0Hz sinusoidal command voltage was applied. (a) Measurement points on the cell. Black points marked by the open circles are measurement points. The measurement points of the microspheres 1 and 10 correspond to those of the apical and basal ends. (b) The axial displacement of the measurement points shown in (a) at the maximum contraction.

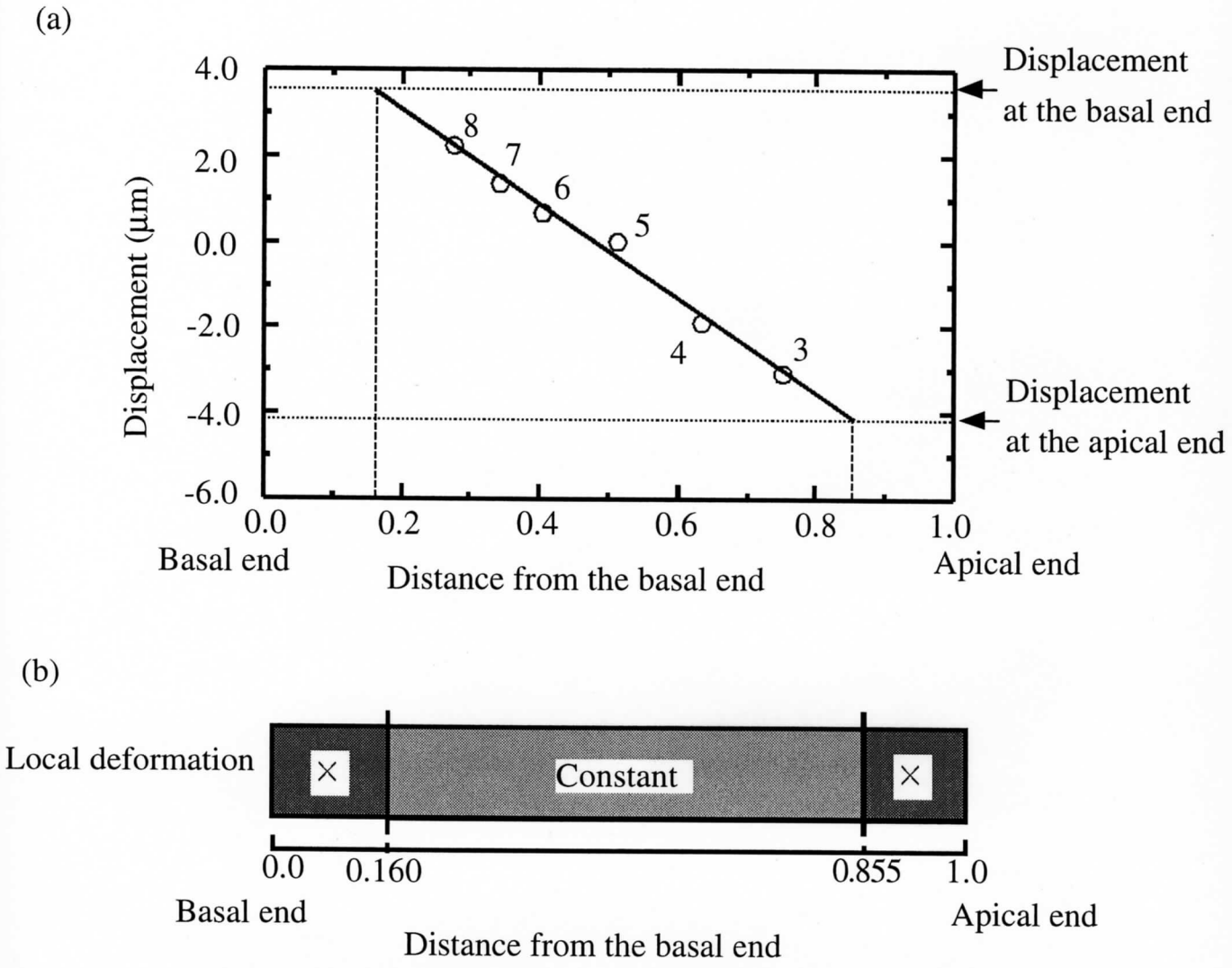

Fig. 3.6. Evaluation of the correlation between the displacement values and the distance along the cell axis. (a) Axial displacements of the measurement points except the apical and basal regions of the cell. The solid line shows a linear regression line given by y=5.30-11.1x; r=0.995. The displacement values obtained from the regression line are equal to that of basal end (3.53μm) at the point 0.160 and that of apical end (-4.18μm) at the point 0.855 from the basal end. This figure shows that the displacement values are proportional to the distance along the cell axis in the region between 0.160 and 0.855 from the basal end and that the displacement values are constant in the region between 0.0 and 0.160 and between 0.855 and 1.0 from the basal end, respectively. (b) The local deformation of the cell. This figure shows that the local deformation is almost constant in the region between 0.160 and 0.855 from the basal end and it does not occur in the region 0 and 0.160 and between 0.855 and 1.0 from the basal end.

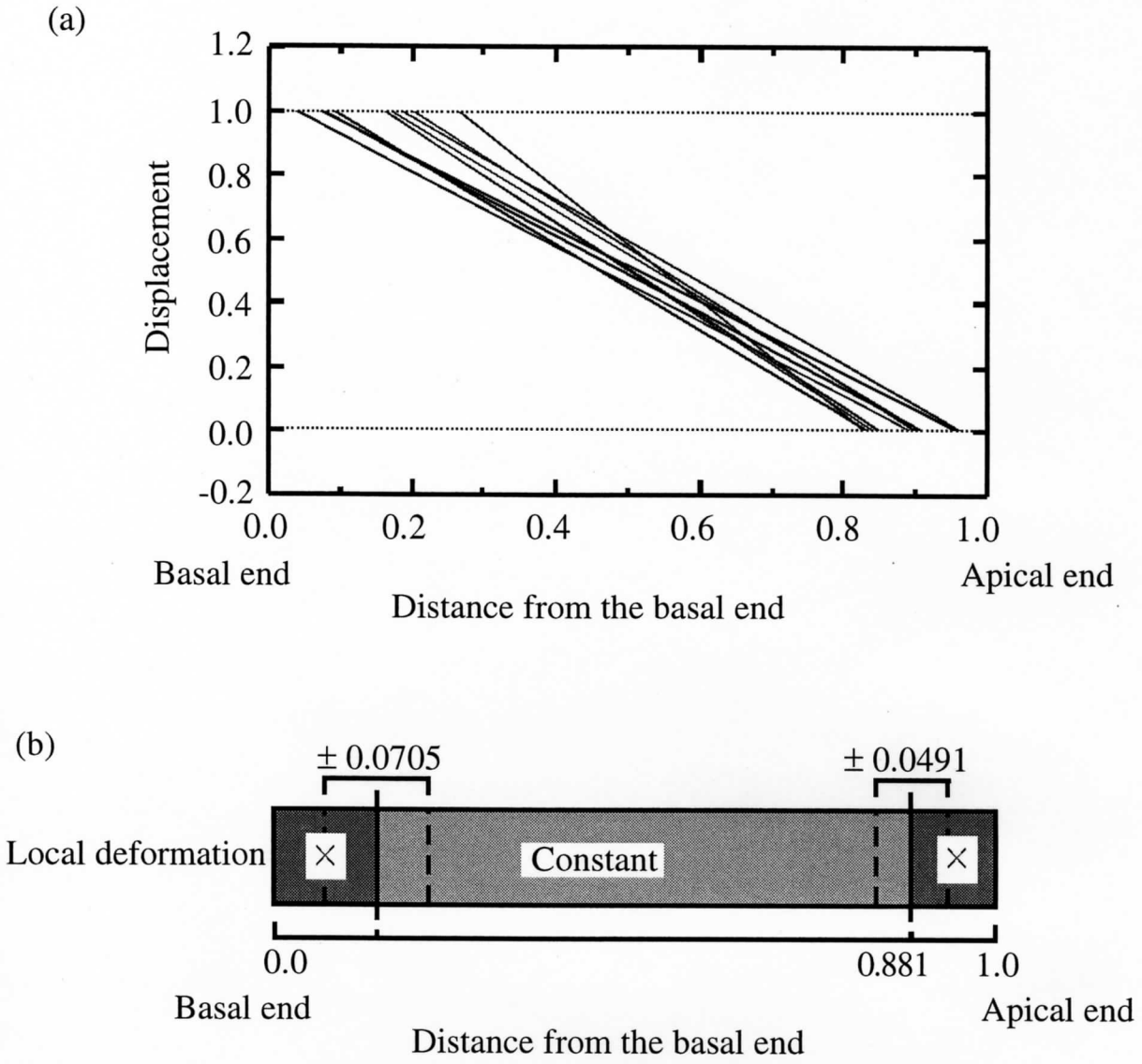

Fig. 3.7. The local deformation evoked by the electric stimulation. (a) Normalized axial displacements of the measurement points except the apical and basal regions of the cell. The solid line shows 10 linear regression lines obtained from the 10 different cells. (b) The local deformation of the cell. Fig. 7(a) shows that the displacement values are proportional to the distance along the cell axis in the region between 0.142±0.0705 (mean±standard deviations) and 0.893±0.0491 from the basal end and that the displacement values are constant to be 1.0 in the region between 0.0 and 0.142±0.0705 and 0.0 in the region between 0.893±0.0491 and 1.0 from the basal end. Fig. 7(b) shows that the local deformation in the middle region of the cell is constant and the local deformation does not occur in the regions between 0.0 and 0.142±0.0705 and between 0.893±0.0491 and 1.0 from the basal end

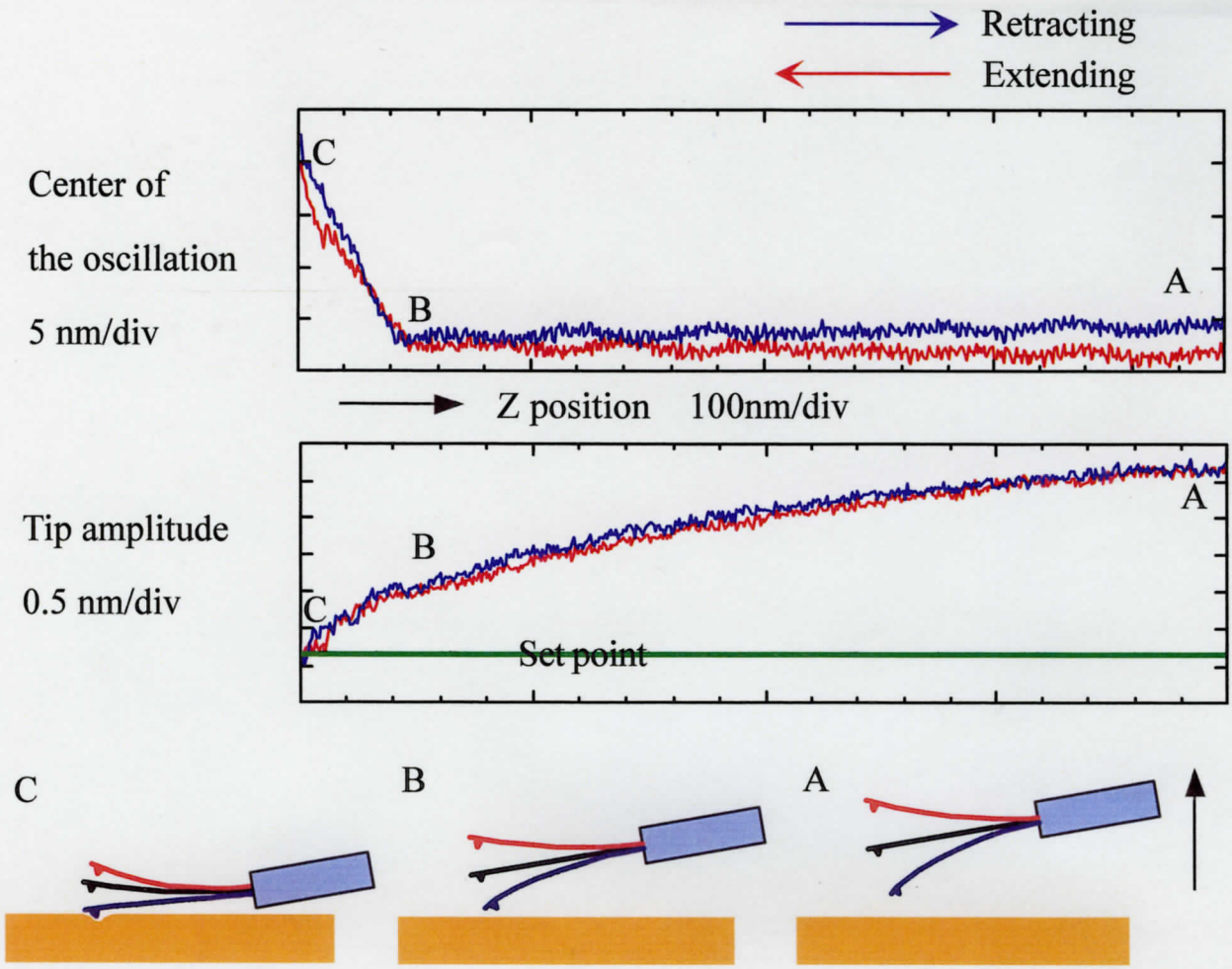

Fig. 3.8. Tip-sample approach curve obtained from OHC. The center of the oscillation and the amplitude of the oscillating tip was plotted against the cantilever position. The red line indicates the curve when the cantilever approached to the OHC surface and the blue line indicates the curve when the cantilever withdrew from the OHC surface. When the oscillating tip was approached to the OHC surface, the amplitude of the oscillating tip decreased by slow degrees in the region between A and B. It is considered that this phenomenon is caused from the viscous resistance of the liquid between the tip and the OHC. In the region between B and C, the amplitude of the oscillating tip decreased and the center of the oscillation shifted upward. This indicates that the tip is contact with the OHC surface and the tip-sample interaction in this region is suited to scanning.

(a)

(b)

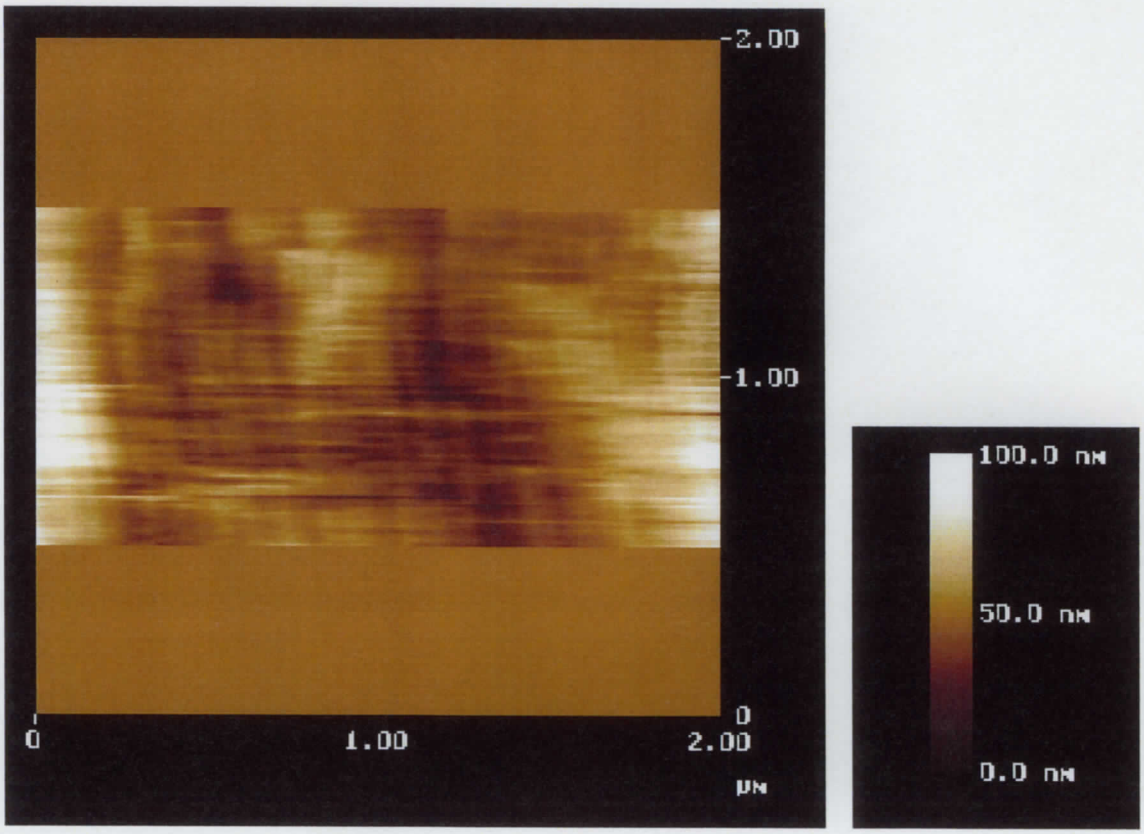

Fig. 3.9. AFM images of the lateral surface in the apical region of the OHC. (a) The position of the scanning area. (b) The AFM image which is scanned at the red area in (a). The scanning area is 1 μm × 2 μm. The filaments which are arranged circumferentially are seen clearly.

(a)

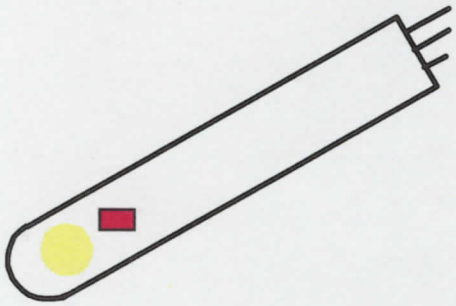

(b)

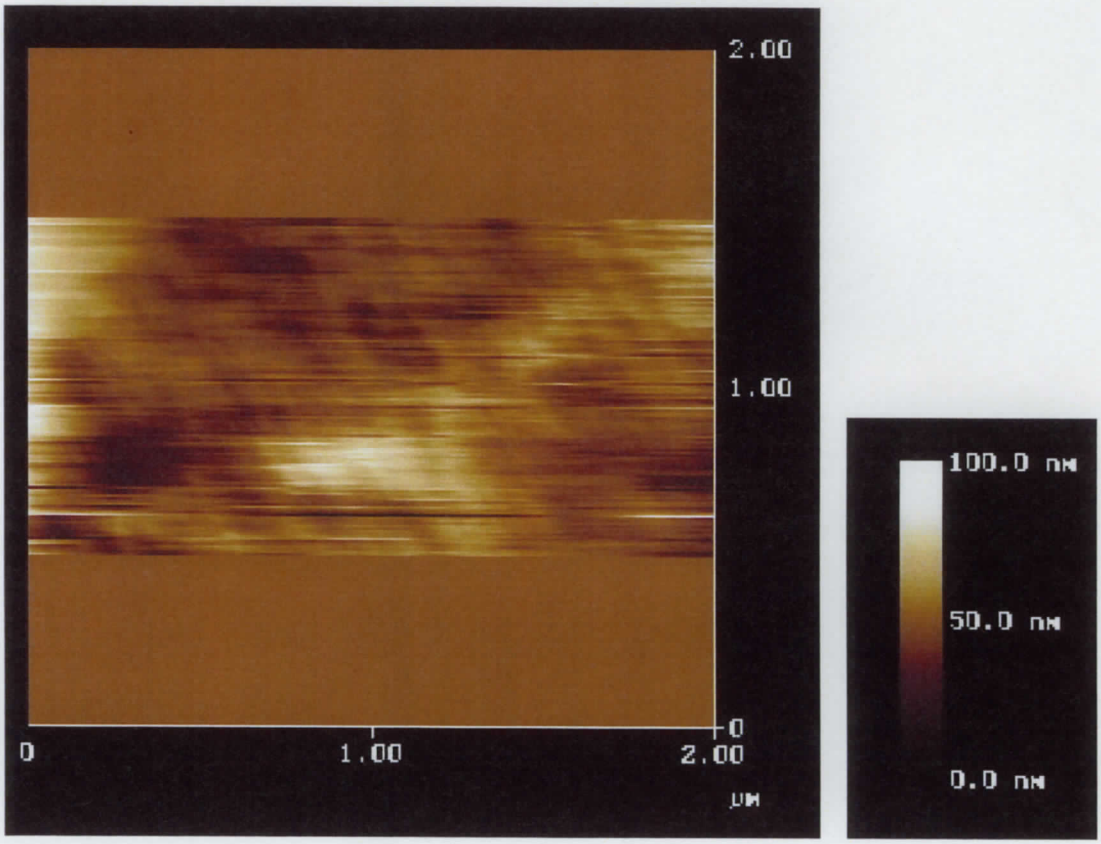

Fig. 3.10. AFM images of the lateral surface in the middle region of the OHC. (a) The position of the scanning area. (b) The AFM image which is scanned at the red area in (a). The scanning area is 1 μm × 2 μm. The filaments which are arranged circumferentially are seen clearly.

(a)

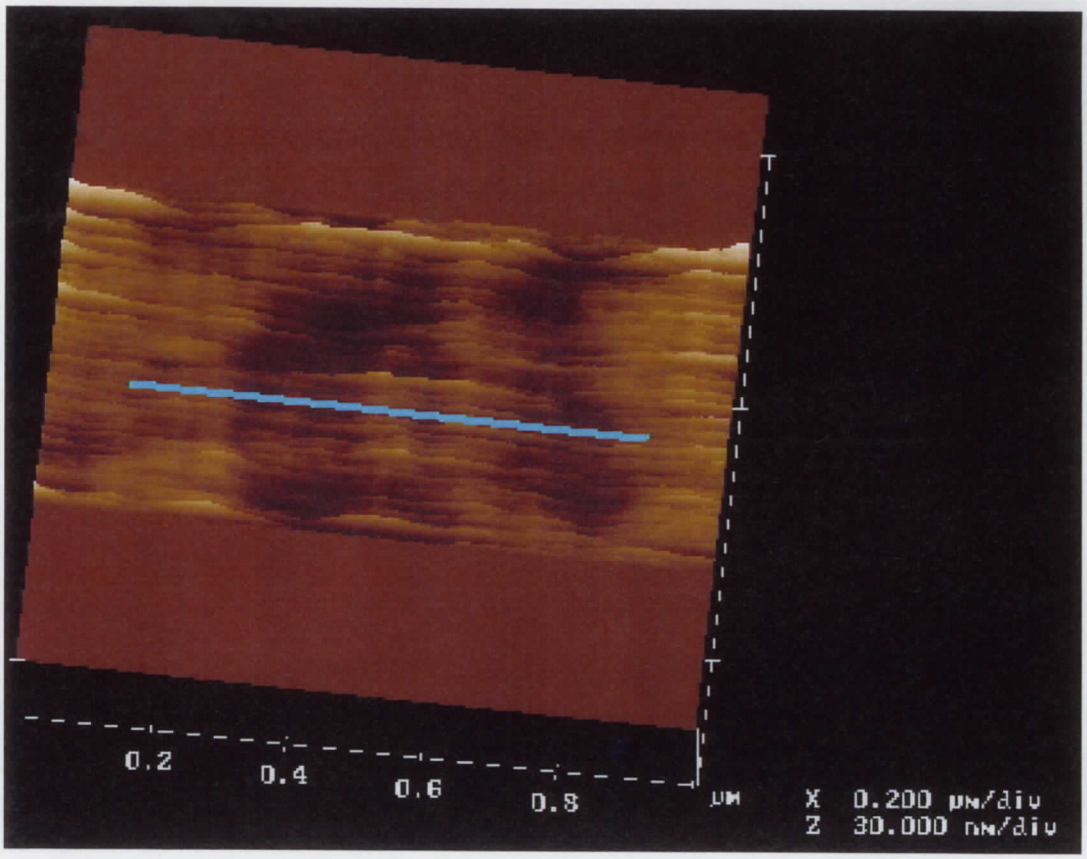

(b)

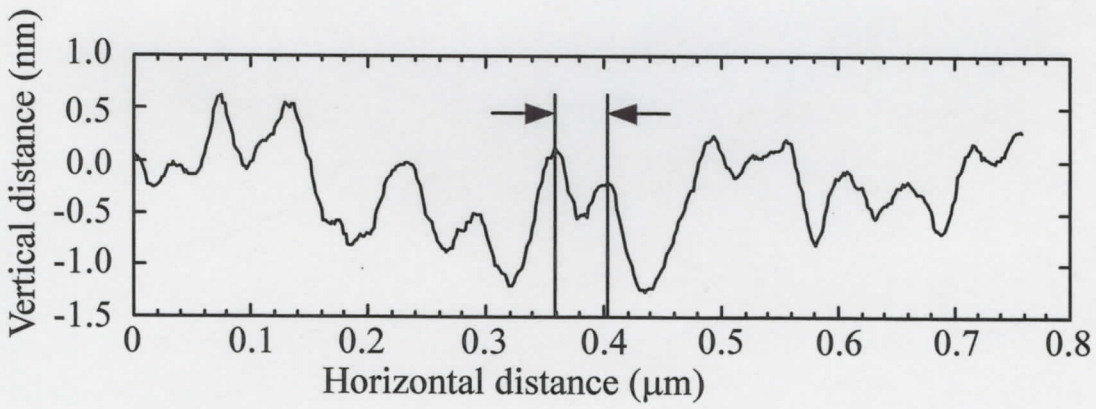

Fig. 3.11. Section analysis. (a) The AFM image of the circumferential filaments. The scanning area is 0.5 μm × 1 μm. (b) The surface profile along the blue line which is shown in (a). In this measurement, the image was sectioned along the blue line which is orthogonal to the direction of the filaments and the surface profile was plotted. From this surface profile, the interval of the circumferential filaments was measured.

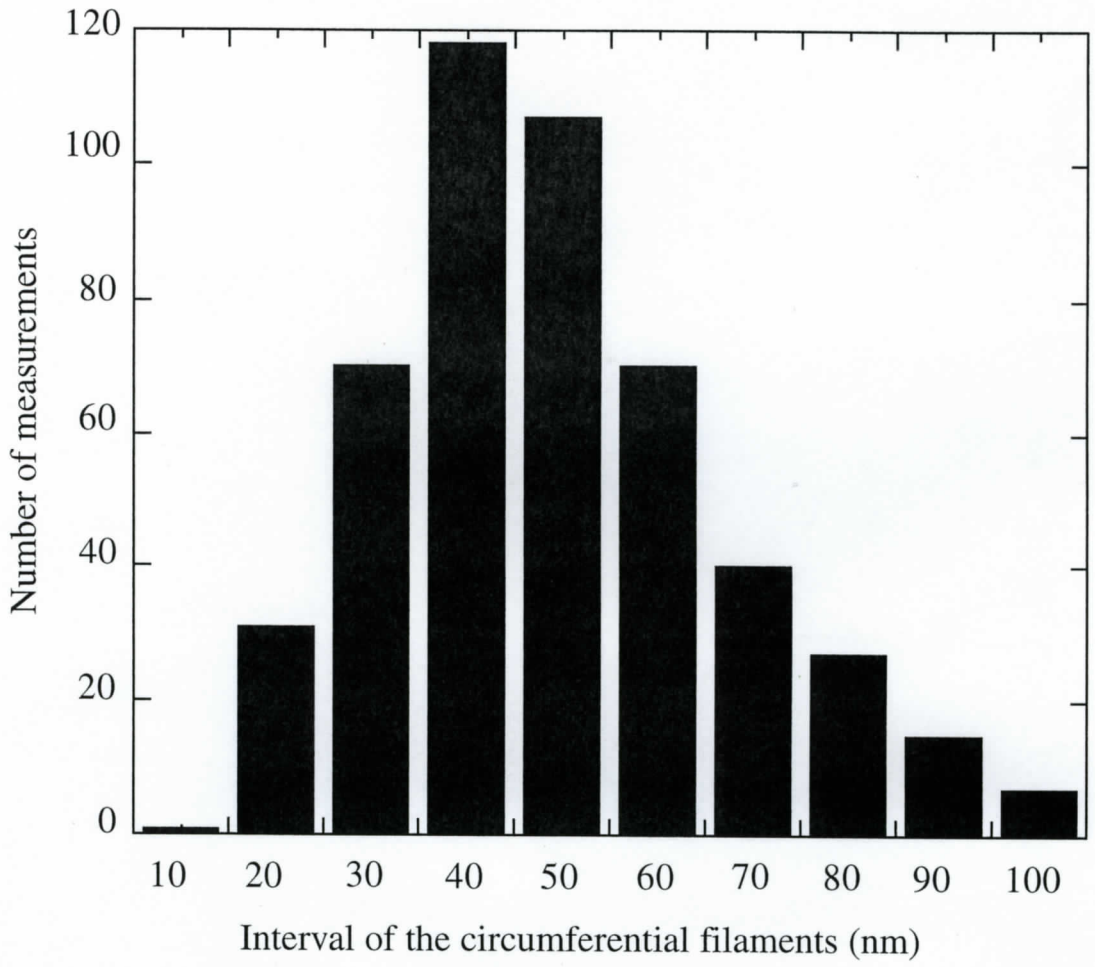

Fig. 3.12. Intervals of the circumferential filaments. The number of measurements is plotted against the interval in 10 nm classes. The interval is ranged from 15 nm to 103 nm and the mean and the standard deviation of them were 49 nm and 18 nm, respectively.

4. Discussion

4.1 The local stiffness of the OHC

When the cell shows the 5% contraction due to the hypotonic stimulation, the local deformation was almost constant in the region between 0.0 and 0.881±0.0447 from the basal end and did not occur in the region between 0.881±0.0447 and 1.0 from the basal end (Fig. 3.3). If the force induced by the increase in the intracellular pressure acts equally on every part of the cell, the difference in the deformation would depend on the stiffness of the cell. Therefore, it is said that the longitudinal stiffness is constant in the region between 0.0 and 0.881±0.0447 from the basal end and the longitudinal stiffness in the region between 0.881±0.0447 and 1.0 from the basal end is higher than other regions. As the microscopic studies reported the existence of the actin surrounding the cuticular plate in the apical part (Slepcky, et al., 1986; Zenner, 1986), it is speculated that the actin will cause high stiffness in the apical part.

4.2 Distribution of the protein motors

When a 5Hz sinusoidal command voltage was applied to the OHC, there is no local deformation in the regions between 0.0 and 0.142±0.0705 and between 0.893±0.0491 and 1.0 from the basal end (Fig. 3.7). Assuming that the local deformation evoked by the electrical stimulation arises from a conformational change of protein motor and that the conformational change of each protein motor is constant, the local deformation evoked by the electrical stimulation would depend on the density of protein motors and the local stiffness of the cell. As it is discussed previously that the longitudinal stiffness is constant in the region between 0.0 and 0.881±0.0447 from the basal end, there would be no motors in the region between 0.0 and

0.142±0.0705 from the basal end. As the local deformation evoked by the electrical stimulation does not occur in the apical region, it is also expected that there are no motors in the region between 0.893±0.0491 and 1.0 from the basal end. However, as the longitudinal stiffness is high in this region, there is another possibility that the apical region has motors but the high stiffness inhibits the apical region from deforming. A further study is necessary to understand the distribution of the protein motors in this region.

On the other hand, the local deformation was almost constant in the region between 0.142±0.0705 and 0.893±0.0491. As the longitudinal stiffness is constant in this region, the local deformation evoked by the electrical stimulation depends on only the density of the protein motors. Therefore, the protein motors would distribute equally along the cell lateral wall in the region between 0.142±0.0705 and 0.893±0.0491 from the basal end (Fig. 4.1).

The microchamber analysis of the OHC motility demonstrated that the local deformation was absent in the regions between 0.0 and 0.2 and between 0.9 and 1.0 from the basal end (Hallworth, et al., 1993). Comparing their data with ours, their no motor region in the basal part is larger than ours. However, both data reveal that the no motor region in the basal part is larger than that in the apical one. As the non-linear capacitance is considered to be accompanied by the conformational change of the protein motor, the measurement of the non-linear capacitance is the other way to know the distribution of the protein motor. Huang, et al. (1993) reported that the basal and apical parts of the OHC were devoid of the non-linear capacitance and the axial length of the no motor regions in the basal and the apical parts are corresponded to about 7μm and 5μm, respectively. As the mean OHC length shown in Figs. 6 and 7 was 52.91μm, the axial length of the no motor regions in the basal and the apical parts obtained from our normalized results corresponded to 7.51±3.73μm and

5.66±2.60μm, respectively, and these results are nearly coincident with the data of Huang, et al. In the microscopic studies of the cell lateral wall, the molecules which are distributed along the plasma membrane are candidates of the protein motor. From the freeze fracture images of the plasma membrane, it was reported that the molecules are distributed along the plasma membrane except the synaptic region and tight junction area (Forge, 1991). This indicates that there are no motors in the apical and basal regions, and our result are consistent with the morphological research.

In this study, the standard deviation values of the no motor or high stiffness regions obtained from the 10 different cells are relatively large (Fig. 4.1). Therefore, there is a question whether these regions correlate with the cell length. Fig. 4.2 shows the relationship between the cell length and the high stiffness or no motor region. The open circles show the points where the displacement value obtained from the each regression lines is equal to 0.0 in Fig. 3.3(a) and the dotted lines indicate the high stiffness regions. The filled circles show the points where the displacement value obtained from the each regression lines is equal to 0.0 or 1.0 in Fig. 3.7(a) and the solid lines indicate the no motor regions. The correlation coefficient r of the linear regression lines, which fit to the open and filled circles were less than 0.40. Therefore, it seems to be no relationship between the cell length and the region where the stiffness is high or the motors are not existed. However, as the cell length shown in Fig. 3.7 is restricted from 47.10μm to 59.10μm, the further data collection from the shorter and longer cells is necessary, in order to clarify the relationship between the cell length and the no motor region.

4.3. Ultrastructure of the OHC lateral wall

When the lateral surface of the fixed OHC was scanned using the AFM tapping mode, the circumferential filaments were observed in every region of the OHC. The

intervals of them were 49 ± 18 nm with the range of 15 - 102 nm. There have been some reports in which the cytoskeleton network was observed in other cells by the AFM imaging of cell's periphery (Henderson et al., 1992; Chang et al., 1993; You et al., 2000). From electron microscopic studies on the OHC lateral wall, it has been demonstrated that the cortical lattice lies beneath the lateral plasma membrane along the full length of the cell and has actins which are arranged circumferentially (Holley and Ashmore, 1988, 1990a, 1990b; Arima et al., 1991). Holley et al. (1992) reported that the mean interval of actins was 61.6 ± 8.0 nm, with a range of 42 - 82 nm in the sectioned cells fixed without extraction. Besides, in the negative stained cells, the actin filaments was observed and the mean interval of them was 56.2 ± 7.3 nm (Holley et al., 1992). As the direction, the distribution and the interval of these filaments are similar to our results, the filaments which were observed in the AFM tapping mode would be actins which are part of the cortical lattice.

It has been reported that the filaments in the cortical lattice formed discrete domains that oriented at various angles to each other (Holley et al., 1992). Filaments ran parallel to each other within a single domain, while individual domains were arranged at different angles to the transverse axis of the cell. Although some circumferential filaments which were observed in the AFM tapping mode were branched off, the domains were not clear in this study. Also the spectrins which cross-link the actin filaments were not observed in this study. One of the reasons why they were not observed is that scanning them is difficult as the spectrins are thinner than the actins. Another reason is as follows: Leonova and Raphael (1999) reported that the spectrins were thin flexible meshwork underlying the actins. If their model of the cortical lattice is correct, there is possibility that only actins are scanned, because the actins and spectrins are different layers. However, in order to discuss it in detail, further study is necessary.

4.4. Relationship between the local stiffness and the ultrastructure

In section 4.1, it was concluded that the longitudinal stiffness of the OHC in the region between 0.881 ± 0.0447 and 1.0 from the basal end is higher than that in the other regions. To discuss the relationship between the local stiffness and the ultrastructure which was observed from the AFM imaging, the intervals of the circumferential filaments were evaluated locally. The intervals of the circumferential filaments in the region between 0.0 and 0.85 and between 0.85 and 1.0 from the basal end are shown in Fig. 4.3. In this figure, to allow a direct comparison, the frequency of measurements in each class is plotted as the percentage of the total number of measurements against the interval in 10 nm classes. The mean intervals of the circumferential filaments in the region between 0.0 and 0.85 and between 0.85 and 1.0 from the basal end were 54 nm and 44 nm, respectively (Table 4.1). The difference in these means was statistically significant for $P<0.05$ using Student's t-test. On the other hand, As shown in Fig. 4.4 and Table 4.2, the mean intervals of the circumferential filaments in the region between 0.0 and 0.4 and between 0.4 and 0.85 from the basal end were 54 nm and 54 nm, respectively and they were not different. These results show that the intervals of the circumferential filaments in the region between 0.85 and 1.0 from the basal end are narrower than that in the region between 0.0 and 0.85 from the basal end.

When the OHC was perfused with the hypotonic solution and the circumferential and longitudinal stress induced by the increase in the intracellular pressure acted on the cell lateral wall, the cell lateral wall showed longitudinal shortening and circumferential extension (Fig. 4.5). As the density of the circumferential filaments is high in the region with the narrow intervals of the circumferential filaments, the circumferential Young's modulus of the cell lateral wall is high in this apical region

of the cell. Therefore, it is expected that the circumferential strain which is evoked by the circumferential stress in the apical region of the cell is smaller than that in the other region. If Poisson's ratio of the cell lateral wall is constant in every region of the cell, the longitudinal strain depends on the circumferential strain. This indicates that the longitudinal strain which is evoked by the circumferential stress in the apical region of the cell is smaller than that in the other region. In this case, as the mean intervals of the circumferential filaments in the regions between 0.0 and 0.85 and between 0.85 and 1.0 from the basal end were 54 nm and 44 nm in our result, the ratio of the longitudinal strain in the apical region of the cell and that in the other region corresponded to 44/54. Therefore, it is expected that the longitudinal strain in the apical region of the cell is 81 % of that in the other region (Fig. 4.6). These results indicate that the high density circumferential filaments in the apical region of the cell is one factor that causes the high stiffness in the apical region of the cell. However, as the local deformation in the apical region of the cell was less than the analytical error when the OHCs showed 5 % shortening of the cell length due to the hypotonic stimulation, it is expected that the difference between the stiffness in the apical region and that in the other regions are large. Therefore it is considered that there are the other factors that cause the high stiffness in the apical region of the cell. One of these factors would be the cuticular plate. The cuticular plate exists in the apical end and it is composed of a dense network of actin filaments. Therefore, it would have a large influence on the circumferential Young's modulus in the apical region of the cell.

In Fig. 4.7, the intervals of the circumferential filaments in the apical region is evaluated in detail. The gray, black, blue and red bars indicate the interval of the circumferential filaments in the region between 0.0 and 0.80, between 0.80 and 0.85, between 0.85 and 0.90, between 0.90 and 0.95 and between 0.95 and 1.0 from the

basal end, respectively. In order to allow direct comparison, the frequency of measurements in each class is plotted as the percentage of the total number of measurements against the interval in 10 nm classes. The mean intervals of the circumferential filaments in the region between 0.0 and 0.80, between 0.80 and 0.85, between 0.85 and 0.90, between 0.90 and 0.95 and between 0.95 and 1.0 from the basal end are 54 nm, 54 nm, 40 nm, 45 nm and 48 nm, respectively (Table. 4.3). From this result, there is a possibility that the intervals of the circumferential filaments in the region between 0.85 and 0.90 is narrowest. This indicates that the stiffness of the OHC in the region between 0.85 and 0.90 would be highest.

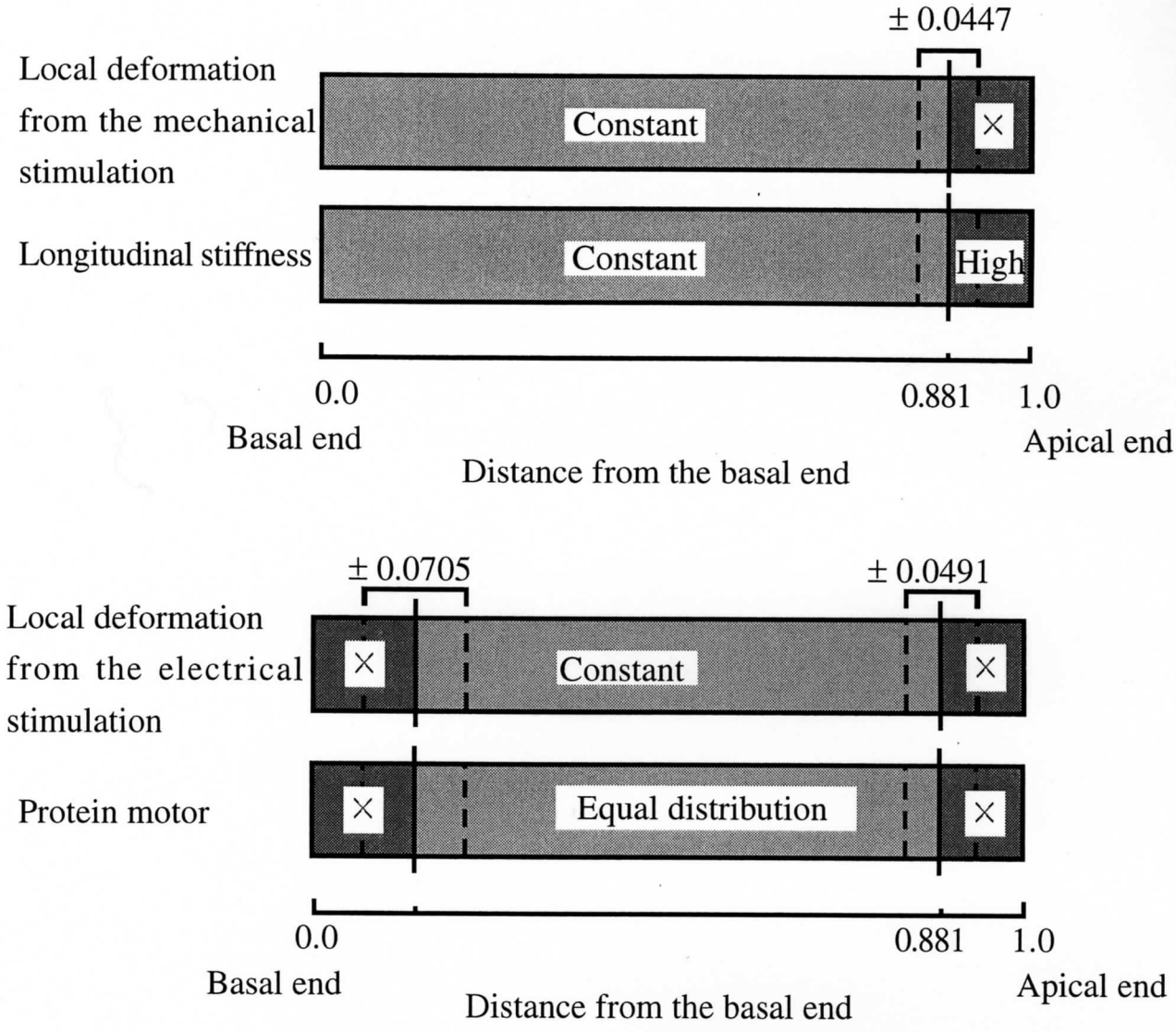

Fig. 4.1. Local stiffness and distribution of protein motor. Assuming that the force induced by the hypotonic stimulation acts equally on every part of the cell, the difference in the deformation depends on the stiffness of the cell. Therefore, it seems that the stiffness is constant in the region between 0.0 and 0.881±0.0447 (mean±standard deviations) from the basal end and the stiffness in the region between 0.881±0.0447 from the basal end is higher than other regions. Moreover, under the assumption that the conformational change of each protein motor is constant, the local deformation which is evoked by electrical stimulation would depend on the density of protein motors and the local stiffness. Therefore, it is said that the protein motors distribute equally along the cell lateral wall in the region between 0.142±0.0705 and 0.893±0.0491 from the basal end and there are no motors in the regions between 0.0 and 0.142±0.0705 and between 0.893±0.0491 and 1.0 from the basal end.

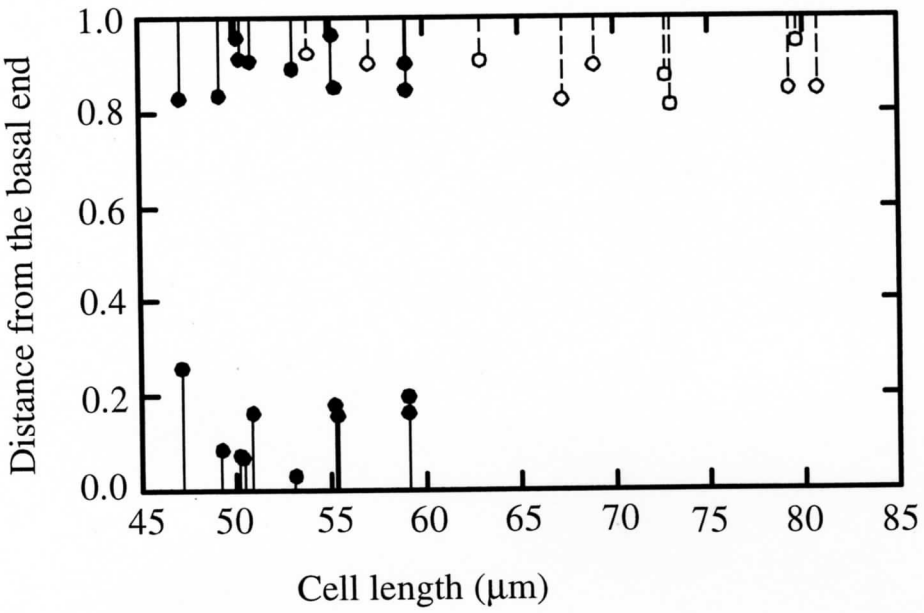

Fig. 4.2. Relationship between the cell length and the high stiffness or no motor region. The open circles show the points where the displacement value obtained from the each regression lines is equal to 0.0 in Fig. 3.3(a) and the dotted lines indicate the high stiffness regions. The filled circles show the points where the displacement value obtained from the each regression lines is equal to 0.0 or 1.0 in Fig. 3.7(a) and the solid lines indicate the no motor regions.

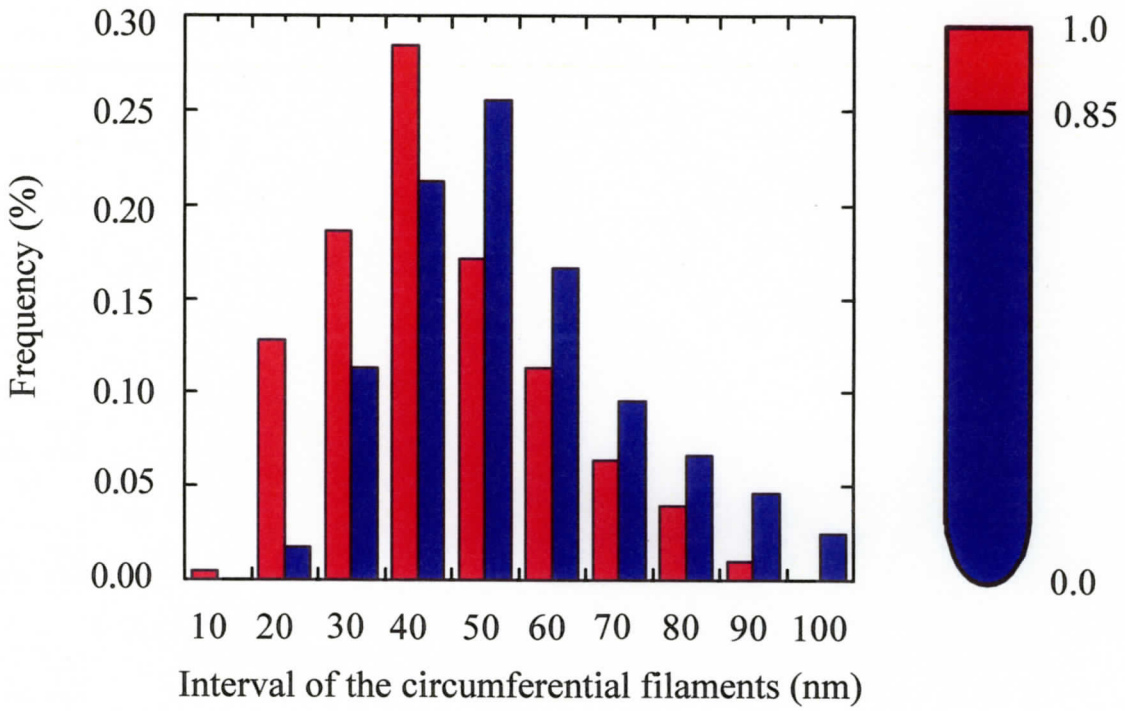

Fig. 4.3. Intervals of the circumferential filaments in the apical region and that in the other region. The blue and red bars indicate the interval of the circumferential filaments in the region between 0.0 and 0.85 and between 0.85 and 1.0 from the basal end, respectively. In order to allow direct comparison, the frequency of measurements in each class is plotted as the percentage of the total number of measurements against the interval in 10 nm classes.

Table. 4.1. Interval of the circumferential filaments.

Region (from the basal end)	Mean (nm)	Standard deviation (nm)	Minimum (nm)	Maximum (nm)	Numbers of measurements
Between 0.0 and 0.85	54	18	18	103	282
Between 0.85 and 1.0	44	17	15	97	204

Mean intervals of the circumferential filaments. The difference in these means was statistically significant for $P<0.05$ using Student's t-test.

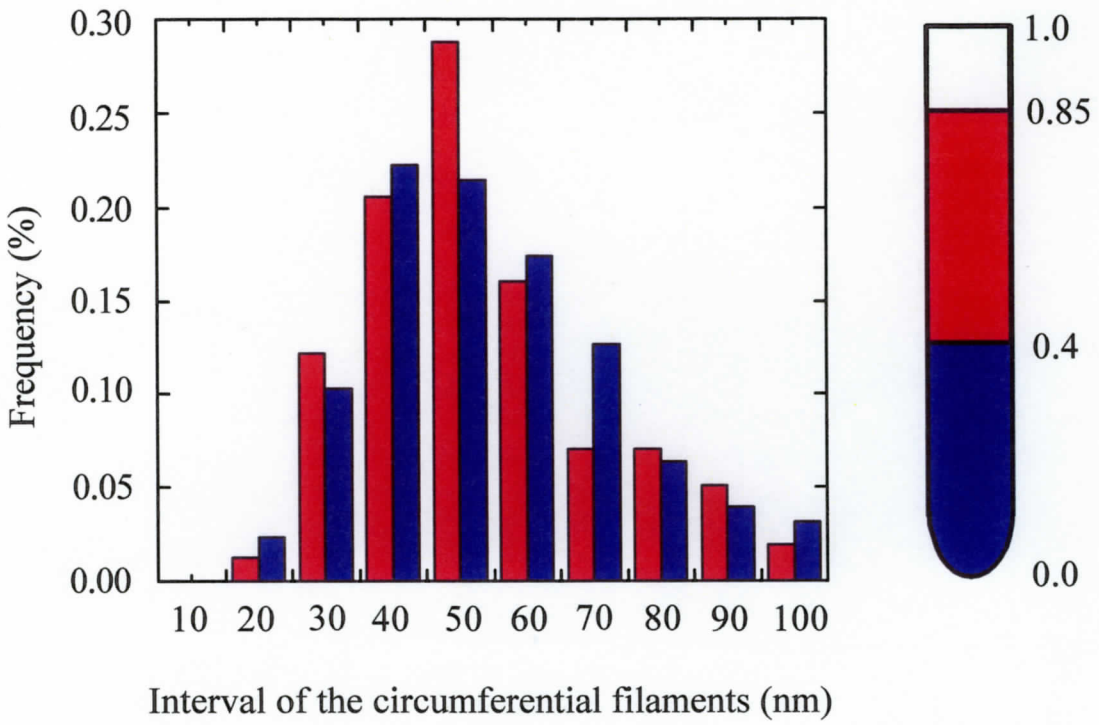

Fig. 4.4. Intervals of the circumferential filaments in the middle and basal regions. The blue and red bars indicate the interval of the circumferential filaments in the region between 0.0 and 0.40 and between 0.40 and 0.85 from the basal end, respectively. In order to allow direct comparison, the frequency of measurements in each class is plotted as the percentage of the total number of measurements against the interval in 10 nm classes.

Table. 4.2. Interval of the circumferential filaments in the middle and basal regions.

Region (from the basal end)	Mean (nm)	Standard deviation (nm)	Minimum (nm)	Maximum (nm)	Numbers of measurements
Between 0.0 and 0.4	54	18	18	103	126
Between 0.4 and 0.85	54	17	21	101	156

The mean intervals of the circumferential filaments in the region between 0.0 and 0.4 and between 0.4 and 0.85 from the basal end were not different.

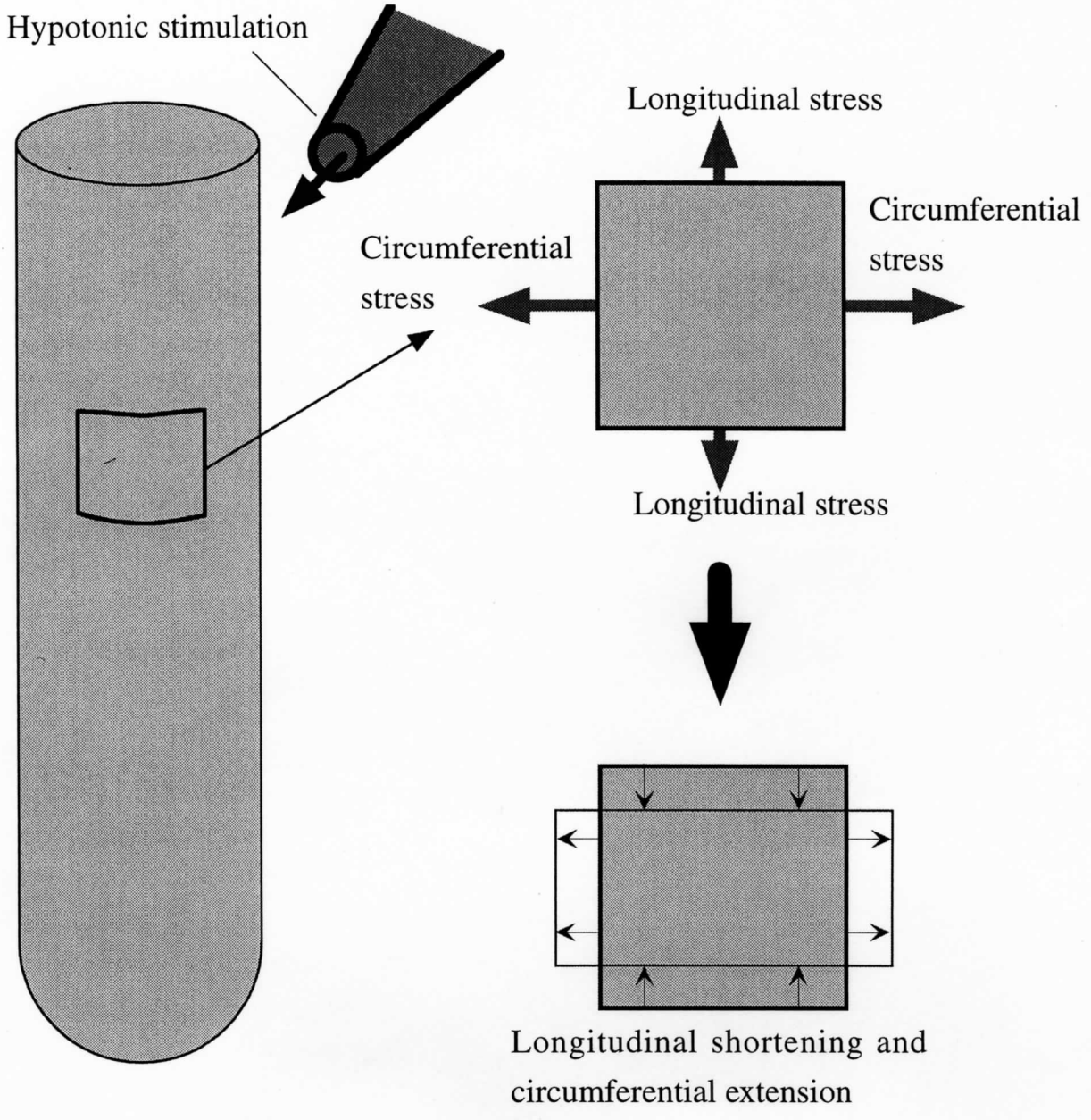

Fig. 4.5. Strain of the cell lateral wall in response to the hypotonic stimulation. When the OHC perfused with the hypotonic solution and the circumferential and longitudinal stresses induced by the increase in the intracellular pressure acted on the cell lateral wall, the cell lateral wall showed longitudinal shortening and circumferential extension.

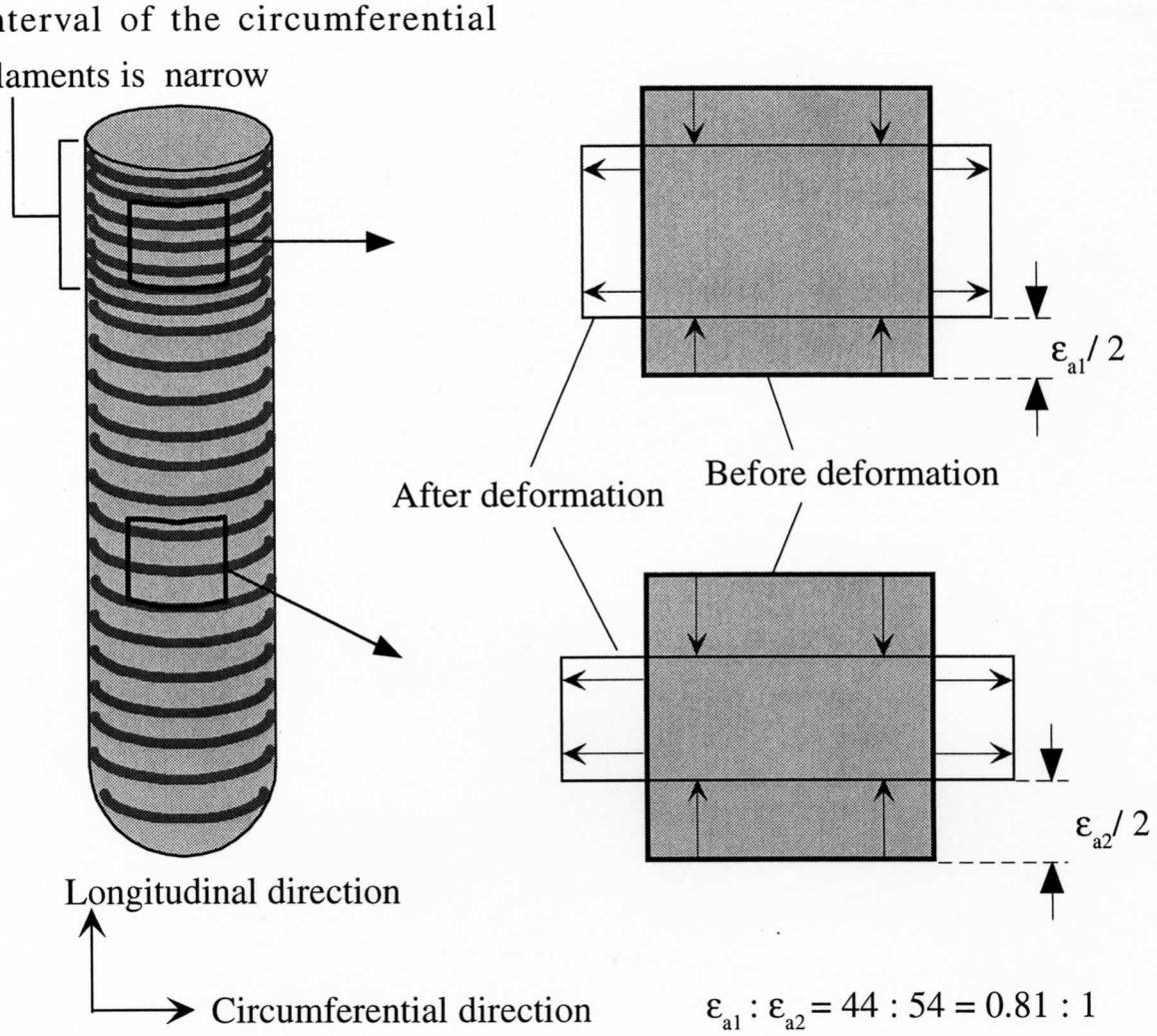

Fig. 4.6. Relationship between the circumferential filaments and the longitudinal strain. As the density of the circumferential filaments is high in the region with the narrow intervals of the circumferential filaments, the circumferential Young's modulus of the cell lateral wall is high in this apical region of the cell. Therefore, it is expected that the circumferential strain which is evoked by the circumferential stress in the apical region of the cell is smaller than that in the other region. If Poisson's ratio of the cell lateral wall is constant in the every region of the cell, the longitudinal strain depends on the circumferential strain. This indicates that the longitudinal strain which is evoked by the circumferential stress in the apical region of the cell is smaller than that in the other region. In this case, as the mean intervals of the circumferential filaments in the regions between 0.0 and 0.85 and between 0.85 and 1.0 from the basal end were 54 nm and 44 nm in our result, the ratio of the longitudinal strain in the apical region of the cell and that in the other region corresponded to 44/54. Therefore, it is expected that the longitudinal strain in the apical region of the cell is 81 % of that in the other region

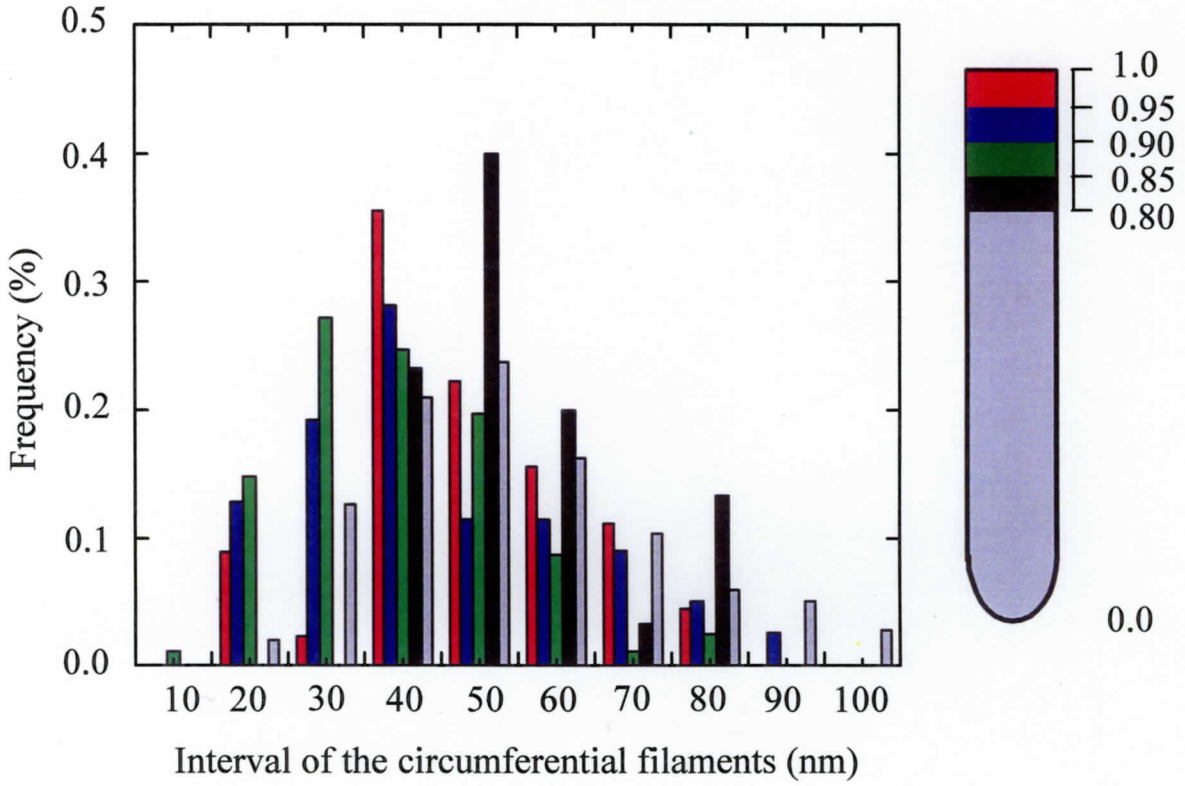

Fig. 4.7. Intervals of the circumferential filaments in the apical region. The gray, black, blue and red bars indicate the interval of the circumferential filaments in the region between 0.0 and 0.80, between 0.80 and 0.85, between 0.85 and 0.90, between 0.90 and 0.95 and between 0.95 and 1.0 from the basal end, respectively. In order to allow direct comparison, the frequency of measurements in each class is plotted as the percentage of the total number of measurements against the interval in 10 nm classes.

Table. 4.3. Interval of the circumferential filaments in the apical region.

Region (from the basal end)	Mean (nm)	Standard deviation (nm)	Minimum (nm)	Maximum (nm)	Numbers of measurements
Between 0.0 and 0.80	54	18	18	103	252
Between 0.80 and 0.85	54	13	35	83	30
Between 0.85 and 0.90	40	16	15	97	81
Between 0.90 and 0.95	45	19	18	94	78
Between 0.95 and 1.0	48	16	20	80	45

There is a possibility that the intervals of the circumferential filaments in the region between 0.85 and 0.90 is narrowest.

4. Conclusions

The local deformation of the OHC in response to the hypotonic and electrical stimulations was analyzed by measuring the displacement of the microspheres attached randomly to the cell lateral wall. Then, the ultrastructure of the OHC lateral wall was investigated by an atomic force microscopy. When the position along the cell axis is represented by the normalized distance from the basal end and the positions of the basal and apical ends are expressed by 0.0 and 1.0, the following conclusions can be drawn.

1. The longitudinal stiffness of the cell is constant in the region between 0.0 and 0.881±0.0447 (mean±standard deviations) from the basal end, and the longitudinal stiffness of the cell in the region between 0.881±0.0447 and 1.0 from the basal end is higher than that in other regions.
2. There are no motors in the regions between 0.0 and 0.142±0.0705 and between 0.893±0.0491 and 1.0 from the basal end, and the motors are distributed equally along the cell lateral wall in the region between 0.142±0.0705 and 0.893±0.0491 from the basal end.
3. The circumferential filaments were observed in the AFM tapping mode, and it would be actins which are part of the cortical lattice.
4. The mean intervals of the circumferential filaments in the region between 0.0 and 0.85 and between 0.85 and 1.0 from the basal end are 54 nm and 44 nm, respectively.
5. The difference between the intervals of the circumferential filaments in the region between 0.0 and 0.85 and between 0.85 and 1.0 from the basal end is one of the factors that cause the high stiffness in the apical region of the cell.

5. References

Arima, T., Kuraoka, A., Toriya, R., Shibata, Y., Uemura, T., 1991. Quick-freeze, deep-etch visualization of the 'cytoskeletal spring' of cochlear outer hair cells. Cell Tissue Res. 263, 91-97.

Ashmore, J. F., 1987. A fast motile response in guinea-pig outer hair cells: the cellular basis of the cochlear amplifier. J. Physiol. 388, 323-347.

Brownell, W. E., Bader, D., Ribaupierre, Y., 1985. Evoked mechanical responses of isolated cochlear outer hair cells. Science 227, 194-196.

Chang, L., Kious, T., Yorgancioglu, M., Keller, D., Pfeiffer, J., 1993. Cytoskeleton of living, unstained cells imaged by scanning force microscopy. Biophys. J. 64, 1282-1286.

Dallos, P., Evans, B. N., 1995. High-frequency motility of outer hair cells and the cochlear amplifier. Science 267, 2006-2009

Evans, B.N., 1990. Fatal contractions: ultrastructural and electromechanical changes in outer hair cells following transmembraneous electrical stimulation. Hear. Res. 45, 265-282.

Forge, A., 1991. Structural features of the lateral walls in mammalian cochlear outer hair cells. Cell Tissue Res. 265, 473-483.

Gale, J.E., 1997. An intrinsic frequency limit to the cochlear amplifier. Nature 389, 63-66.

Hallworth, R., Evans, B. N., Dallos, P., 1993. The location and mechanism of electromotility in guinea pig outer hair cell. J. Neurophysiol. 70, 549-558.

Hallworth, R., 1995. Passive compliance and active force generation in the guinea pig outer hair cell. J. Neurophysiol. 74, 2319-2329.

Henderson, E., Haydon, P. G., Sakaguchi, D. S., 1992. Actin filament dynamics in living gliai cells imaged by atomic force microscopy. Science 257, 1944-1946.

Holley, M. C., Ashmore, J. F., 1988a. A cytoskeletal spring in cochlear outer hair cells. Nature 335, 635-637.

Holley, M. C., Ashmore, J. F., 1988b. On the mechanism of a high-frequency force generator in outer hair cells isolated from the guinea pig cochlea. Proc. R. Soc. Lond. B 232, 413-429.

Holley, M. C., Ashmore, J. F., 1990a. Spectrin, actin and the structure of the cortical lattice in mammalian cochlear outer hair cells. J. Cell. Science 96, 283-291.

Holley, M. C., Ashmore, J. F., 1990b. A cytoskeletal spring for the control of cell shape in outer hair cells isolated from the guinea pig cochlea. Eur Arch Otorhinolaryugol 247, 4-7.

Holley, M. C., Kalinec, F., Kachar, B., 1992. Structure of the cortical cytoskeleton in mammalian outer hair cells. J. Cell. Science 102, 569-580.

Huang, G., Santos-Sacchi, J., 1993. Mapping the distribution of the outer hair cell motility voltage sensor by electrical amputation. Biophys. J. 65, 2228-2236.

Huang, G., Santos-Sacchi, J., 1994. Motility voltage sensor of the outer hair cell resides within the lateral plasma membrane. Proc. Natl. Acad. Sci. USA 91, 12268-12272.

Kachar, B., Brownell, W. E., Altschuler, R., Fex, J., 1986. Electrokinetic shape changes of cochlear outer hair cells. Nature 322, 365-368.

Kalinec, F., Holley, M. C., Iwasa, K. H., Lim, D. J., Kachar, B., 1992. A membrane-based force generation mechanism in auditory. Proc. Natl. Acad. Sci. USA 86, 8671-8675.

Leonova, E. V., Raphael, Y., 1999. Application of a platinum replica method to study of the cytoskeleton of isolated hair cells supporting cells and whole mounts of the organ of Corti. Hear. Res. 130, 137-154.

Putman, C. A. J., Van der Werf, K. O. J., De Grooth, B. G., Van Hulst, N. F., Greve, J., 1994. Tapping mode atomic force microscopy in liquid. Appl. Phys. Lett. 64, 2454-2456.

Saito, K., 1983. Fine structure of the sensory epithelium of guinea-pig organ of

Corti: Subsurface cisternae and lamellar bodies in the outer hair cells. Cell Tissue Res. 229, 467-481.

Santos-Sacchi, J., Dilger, J. P., 1988. Whole cell currents and mechanical responses of isolated outer hair cells. Hear. Res. 35, 143-150.

Santos-Sacchi, J., 1990. Fast outer hair cell motility: How fast is fast? In: Dallos, P., Geisler, C. D., Matthews, J. W., Ruggero, M. A., Steele, C. R. (Eds.), The Mechanics and Biophysics of Hearing. Springer-Verlag, Berlin, pp. 69-75.

Santos-Sacchi, J., 1991. Reversible inhibition of voltage-dependent outer hair cell motility and capacitance. J. Neurosci. 11, 3096-3110.

Santos-Sacchi, J., 1992. On the frequency limit and phase of outer hair cell motility: effects of the membrane filter. J. Neurosci. 12, 1906-1916.

Slepecky, N., Chamberlain, S. C., 1986. Correlative immuno-electron-microscopic and immunofluorescent localization of actin in sensory and supporting cells of the inner ear by use of a low-temperature embedding resin. Cell Tissue Res. 245, 229-235.

You, H. X., Lau, J. M., Zhang, S., Yu, Lei., 2000. Atomic force microscopy imaging of living cells: a preliminary study of the disruptive effect of the cantilever tip on cell morphology. Ultramicroscopy 82, 297-305.

Zenner, H. P., 1986. Motile responses in outer hair cells. Hear. Res. 22, 83-90.

Zenner, H. P., Gitter, A. H., Rudert, M., Ernst, A., 1992. Stiffness, compliance, elasticity and force generation of outer hair cells. Acta Otolaryngol. (Stockh.) 112, 248-253.

Zheng, J., Shen, W., He, D. Z. Z., Madison, L. D., Dallos, P., 2000. Prestin is the motor protein of cochlear outer hair cells. Nature 405, 149-155.